NUMERICAL MODELING OF SEQUENTIAL SEGMENTATION FOR ENHANCEMENT OF MIXING INSIDE MICROCHANNELS.

by

Ibragim Abu Dagga

A Thesis presented to the Faculty of the
American University of Sharjah
College of Engineering
In Partial Fulfillment
of the Requirements
for the Degree of

Master of Science in
Mechanical Engineering

Sharjah, United Arab Emirates
December 2019

Approval Signatures

We, the undersigned, approve the Master's Thesis of Ibragim Abu Dagga.

Thesis Title: Numerical Modeling of Sequential Segmentation for Enhancement of Mixing Inside Microchannels.

Signature	**Date of Signature** (dd/mm/yyyy)
_____	_____
Dr. Mohamed Abdelgawad Associate Professor, Department of Mechanical Engineering Thesis Advisor	
_____	_____
Dr. Mohammad Omar Hamdan Associate Professor, Department of Mechanical Engineering Thesis Committee Member	
_____	_____
Dr. Rachid Chebbi Professor, Department of Chemical Engineering Thesis Committee Member	
_____	_____
Dr. Mamoun Abdel-Hafez Head, Department of Mechanical Engineering	
_____	_____
Dr. Lotfi Romdhane Associate Dean for Graduate Affairs and Research College of Engineering	
_____	_____
Dr. Naif Darwish Acting Dean, College of Engineering	
_____	_____
Dr. Mohamed El-Tarhuni Vice Provost for Graduate Studies	

Acknowledgment

I take this momentous opportunity to express my heartfelt gratitude and full respect to my great supervisor Dr. Mohamed Abdelgawad who taught, encouraged, and put all of his effort to give me his guidance throughout my research stages. I'm deeply beholden for his great assistance, worthy discussion and suggestions.

I would like to thank the professors of the Mechanical and Chemical Engineering departments who taught me the master level courses with mighty teaching methods and skills. I am really appreciate of their dignified advices and motivation. I would like to thank especially Dr. Mohammad Omar Hamdan and Dr. Rachid Chebbi for their helpful and detailed comments.

I would like to acknowledge the American University of Sharjah for granting me a full assistantship for the master's program.

Abstract

Microfluidics appeared recently as a new tool that facilitates many applications including chemical synthesis, electronics cooling and biological assays. However, flow on the microscale is characterized by laminar flow which renders mixing a challenge and reduces the effectiveness of mixing in many applications. Therefore, many techniques have been reported to enhance mixing inside microchannels. This thesis demonstrates the different mixing techniques inside microchannels and investigates sequential segmentation as an active mixing technique. In sequential segmentation, the solute and the solvent are divided into segments in the axial direction. Due to the parabolic velocity profile exhibited in laminar flow, Taylor-Aris dispersion can improve mixing by several orders of magnitude as compared with pure molecular diffusion. The present work comprises a comprehensive study to optimize this technique. A numerical model was built using COMSOL Multiphysics to calculate the concentration distribution by diffusion and advection in the entire microchannel. The different investigated parameters that were optimized are frequency, flow velocity, duty cycle (DC), aspect ratio, cross-sectional shape, and effect of inlet configuration of inlet branches. It has been found that changing the channel aspect ratio has the most significant effect on mixing efficiency. The analysis of aspect ratio (H:W) showed a moderate increase in mixing index for aspect ratio of 4:1. However, an aspect ratio of 1:4 is extremely inefficient. The best mixing efficiency achieved is that of sequential segmentation coupled with hydrodynamic focusing which is 99.7%. On the contrary, changing the shape of inlet branches to T-shape or arrow-head shape decreased the mixing index. Increasing segmentation frequency was found to increase the mixing efficiency up to a frequency of 150 Hz beyond which mixing efficiency decreased due to non-complete segmentation of both streams at higher frequencies. The duty cycle effect is mainly important for specific microfluidic applications that require different mixing fractions of the solutions. It is shown that by increasing the duty cycle of the solvent, mixing slightly increases, whereas decreasing it leads to a reduction in mixing. The effect of different cross-sectional shapes also has a small effect on the mixing index.

Keywords: ***micromixer; sequential segmentation; microfluidic; chemical synthesis, microchannel.***

Table of Contents

List of Figures

List of Tables

Chapter 1. Introduction

Microfluidics is the science that deals with the manipulation and precise control of fluids on the microscale, which is usually done in networks of microchannels. Through miniaturization, one can improve the precision of experiments, decrease sample and reagent consumption, run multiple analyses simultaneously and reduce the overall costs of applications. Over the past three decades, miniaturization through lab-on-a-chip technology was used successfully in various application such as chemical synthesis [1, 2], cell assays [3, 4], proteomics [5], immunoassays [6], and point of care diagnostics [7].

Chemical synthesis in particular benefited a lot from miniaturization advantages by Lab-on-chip devices. Continuous flow reactions in microchannels were reported for synthesis of colloidal silica [1], nanoparticles [2, 8, 9], peptides [10], and nanocrystals [11]. Currently, microflow chemistry is an emerging branch that attracts a lot of attention because of the homogenous reaction conditions it provides and reproducibility of reaction kinetics unlike batch-wise production.

Although miniaturization brings many advantages with it, it also brings with it its own challenges that do not usually occur on the macroscales. For example, laminar flow that is caused by the viscous effects on the microscale makes turbulence based mixing impractical. Therefore, molecular diffusion is considered the main mixing mechanism on the microscale and a variety of micromixing techniques were developed to improve molecular diffusion either through increasing number of contact areas or by reducing the mixing length scale. Consequently, micromixers were applied to a wide range of applications, such as: organic synthesis that is widely applied in drug discovery, crystallization with its important role in catalyst design, and nanoparticle synthesis for encapsulated drug delivery [12].

Understanding the fundamentals of different transport phenomena's on the microscale is essential for the design of effective micromixers rather than just scaling down the macroscale mixing device. Micromixers can be categorized into passive or active depending on the mixing mechanism. Passive mixing depends mainly on enhancing molecular diffusion whereas active mixing uses external sources to disturb the flow and enhance mixing. Generally, the laws that describe flow at a macroscale are the same for microscale flow. However, moving from the macro to micro scale

brings with it additional characteristics that can give different advantages to perform new type of processes that were not possible in the macroscale.

1.1 Diffusion and Advection.

Diffusion transport happens due to the random motion of molecules. It is defined as the process of moving molecules from a region of higher concentration to a one with lower concertation, also called the Brownian motion [13]. Mixing rate can be determined by the diffusional flux j as described in equation 1, which is also known as Fick's law of diffusion [13].

$$j_A = -\rho D_{AB} \nabla \omega_A \tag{1}$$

where ρ is the density in kg/m^3, D_{AB} is the diffusion coefficient in m^2/s and ω_A is the mass fraction of species A. The diffusion coefficient in diluted liquids, with large spherical molecules is described by Stokes-Einstein equation as [13]:

$$D_{AB} = \frac{kT}{6\pi\mu R} \tag{2}$$

where k is the Boltzmann constant, T is the absolute temperature, μ is the dynamic viscosity and R is the radius of molecule. In general the diffusivity will be a function of pressure, temperature and composition [13].

The mass flux can also be caused by advection, where the convection is happening through the bulk flow and it is described as:

$$j_{conv} = \mathbf{v}c \tag{3}$$

where **v** represents the velocity vector in three-dimensions. The three-dimensional diffusion/advection transport that describes the mass flux balance equation is:

$$\frac{\partial c}{\partial t} + u\frac{\partial c}{\partial x} + v\frac{\partial c}{\partial y} + w\frac{\partial c}{\partial z} = D\left(\frac{\partial^2 c}{\partial x^2} + \frac{\partial^2 c}{\partial y^2} + \frac{\partial^2 c}{\partial z^2}\right) + r \tag{4}$$

where u, v, and w are the velocity components in x, y, and z direction. The first term on the left side of (eq. 4) represents the transient change of the concentration, the other three terms on the left represents the advection. The first term on the right side represents the diffusive mass flux. The last term r is the chemical reaction source that describes the generation of the solute.

1.2 Taylor-Aris Dispersion.

Pressure-driven flows inside a microchannel will produce an evenly distributed velocity profile across the channel. “The convective transport at the fluid layers with different velocities causes an apparently higher axial dispersion than pure molecular diffusion” [14] as shown in Figure 1. When the concentration (black) diffuses out in the transverse direction (green), the parabolic velocity profile (red) changes the shape of the concentration, because of the changing velocity in the transverse direction (blue). This raises an extra spread of the concentration in the x-direction.

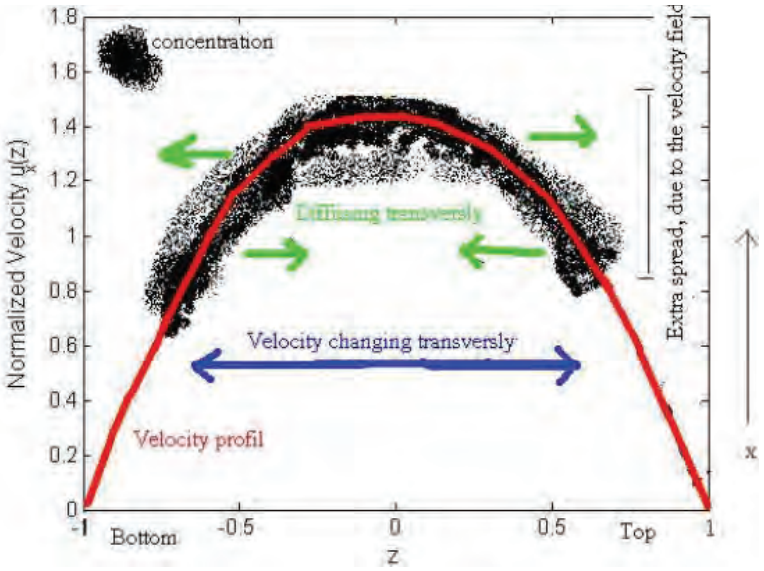

Figure 1 Sketch of Taylor-Aris dispersion for a point concentration placed in the center. Due to the velocity field an extra amount of spreading can be seen [14].

For a cylindrical capillary, the asymptotic solution for the axial dispersion of a cylindrical capillary can be described as [15, 16]:

$$D^* = D\left[1 + \frac{1}{48}Pe(r)^2\right] \tag{5}$$

where $Pe(r)$ is the Peclet number based on the radius r. As discussed in the appendices, Peclet number in microfluidic applications may reach 100,000, which is going to make the axial dispersion coefficient D^* of several order of magnitude higher than molecular diffusion coefficient D. Whereas for the flow between two parallel plates with a distance of H in between, the dispersion coefficient is [17]:

$$D^* = D\left[1 + \frac{1}{210} Pe_H^2\right] \tag{6}$$

where $Pe_H$is the Peclet number based on the height H between the plates. The dispersion coefficient for a rectangular channel of height H and width W is described as [17]:

$$D^* = D\left[1 + \frac{1}{210}\, Pe_W^2 f\left(\frac{H}{W}\right)\right] \tag{7}$$

where Pe_w is the Peclet number based on the channel width and the aspect ratio height/width.

Chapter 2. Literature Review of Micromixers

As mentioned above micromixers can be classified into two types: passive and active [18]. Passive micromixers do not use moving parts and actuators; rather the mixing process only based on molecular diffusion and chaotic advection. Chaotic advection concept is more feasible for mixing of large molecules with small diffusion coefficients. Passive mixers can be also categorized based on the arrangement of the two solutions to be mixed as serial lamination, parallel lamination, sequential segmentation and injection.

On the other hand, active micromixers use external energy sources as an input and fluid pumping energy to introduce time dependent perturbations that stir the fluid to accelerate the mixing process. It is categorized based on the source of the energy disturbance, which can be electrohydrodynamic, dielectrophoretic, electrokinetic, magneto-hydrodynamic, acoustic, or even based on induced pressure and/or temperature variations. In general, active micromixers have higher mixing efficiency [19]. However, the extra fabrication required and additional energy consumption by these active micromixers makes them difficult to integrate and less attractive in practical applications [20].

2.1 Passive Micromixers

Passive micromixing concepts rely only on molecular diffusion transport and chaotic advection. The passive mixers channel geometry is designed in a way that decreases the diffusion path and increases the surface area between the different solutions. The same concept is applicable in the chaotic advection, where the enhancement comes by changing the design to create new manipulation techniques for laminar flow inside of the microchannel. The basic passive micromixer concepts for decreasing the diffusion path inside of the channel are Parallel lamination, sequential lamination, focusing enhancement, chaotic advection, and multiphase micromixers.

2.1.1 T or Y shaped micromixers. The most basic design of a micromixers is a T shaped or Y shaped channel, where the mixing happens by guiding the two liquids coming from separate inlet ports and merging them to flow adjacently inside of the microchannel. A schematic of a T-shaped micromixer is shown in Figure 2, where mixing solely depends on diffusion of the species at the interface between two liquids.

Consequently, mixing is slow and an unacceptably long channel is required that cannot be used in many applications.

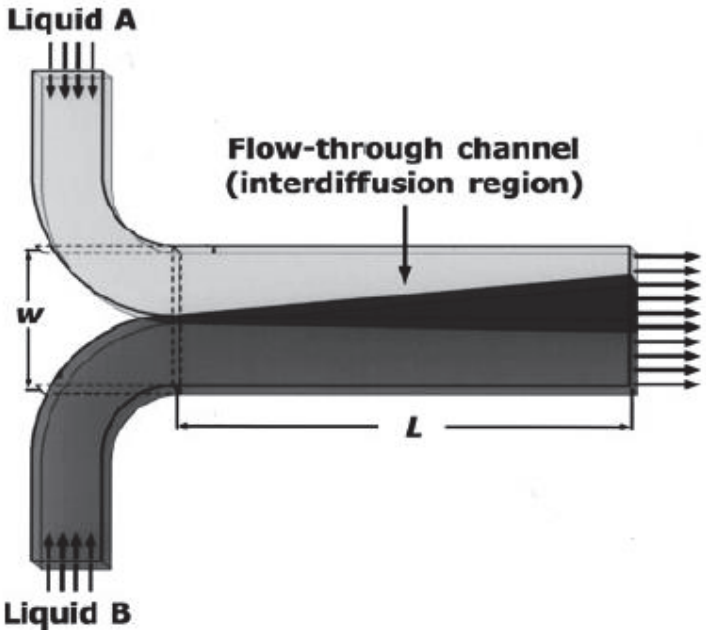

Figure 2 Flow through the T- Shaped micromixer, with each solution containing a different species. L represents the length of the channel and w represents the width [21].

2.1.2 Parallel lamination. In parallel lamination, the inlet main streams are split into *n* pairs to reduce the mixing length. For example, a simple T shaped micromixer with two streams, a mixing length L_{mixing} and a width of W, should have a residence time similar to the average diffusion time:

$$t_{res} = t_{diff} \tag{8}$$

$$\frac{L_{mixing}}{U} = \frac{Fo\ L_{mixing}^2}{D} = \frac{FoW^2}{D} \tag{9}$$

Therefore the ratio between the channel length and width is:

$$\frac{L_{mixing}}{W} = \frac{Fo\ UW}{D} = FoPe_w \tag{10}$$

If the inlets main streams of the basic T or Y shaped micromixer are split as n pairs of solute-solvent streams and rejoined later in a single stream (Figure 3), the mixing length will be reduced to $L_{mixing} = W/n$. Thus, the ratio of the required channel length and width then becomes:

$$\frac{L_{mixing}}{W} = \frac{Fo\ UW}{D} = \frac{1}{n^2} Fo\ Pe_w \tag{11}$$

So "by subdividing each stream into n laminae leads to mixing that is faster by a factor of n^2" [22].

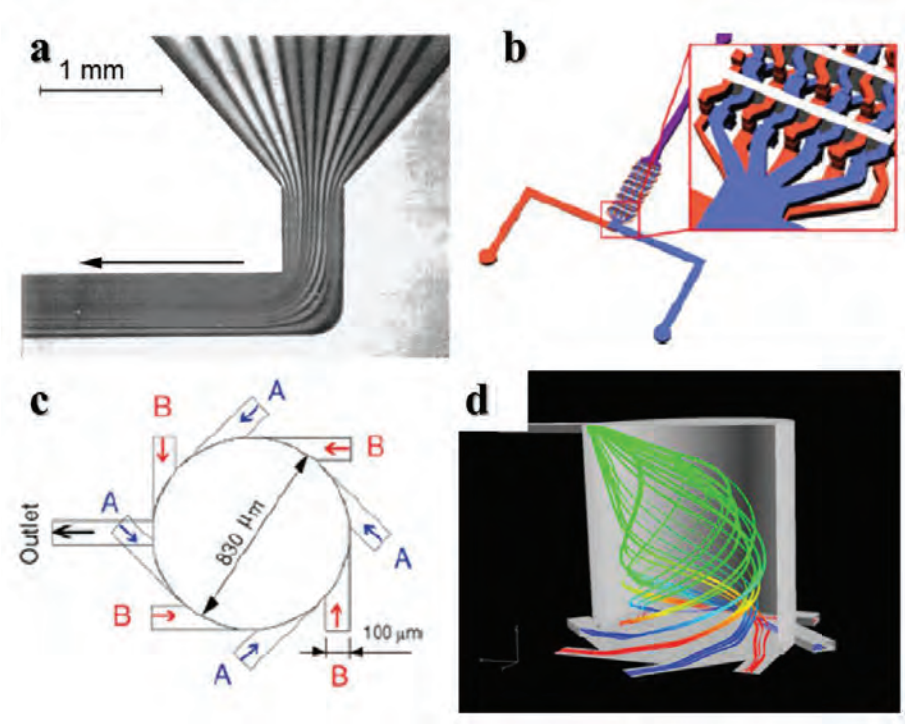

Figure 3 parallel lamination micromixer: (a) Bifurcation-type feeds [22] (b) Circular micromixer [23]. (c, d) A 3D Chessboard micromixer top and side view (d) [24].

2.1.3 Sequential lamination. Sequential lamination micromixers separate the inlet stream into two channels and rejoins them, this process can be repeated many times to increase the contact area between the layers as in parallel lamination. "Sequential laminations is also called split and recombine (SAR) micromixers" [25]. This method relies on an exponential increase in the contact surface area between the

solutions and decrease in the length path to reach a good mixing within a short mixing time.

Using n number of transformation stages in serial, one can laminate 2^n layers, which will make the mixing 4^n times faster. Where if the inlets in the microchannel are stretched and folded n number of cycles, the mixing length is further reduced to $L_{mixing} = W/b^n$. The base b will depend on the type of mixer. For an example, in case of sequential lamination the base b = 2. It could have a different value if it has a chaotic advection. Thus, the required ratio between the channel length and width is going to be:

$$\frac{L_{mixing}}{W} = \frac{1}{b^{2n}} Fo\ Pe_w \tag{12}$$

Equation (12) indicates that a very compact micromixer can be developed using sequential lamination or chaotic advection [26]. However, in order to achieve this sequential lamination mixing, three steps should be followed: flow splitting, flow recombination, and flow rearrangement as illustrated in Figure 4.

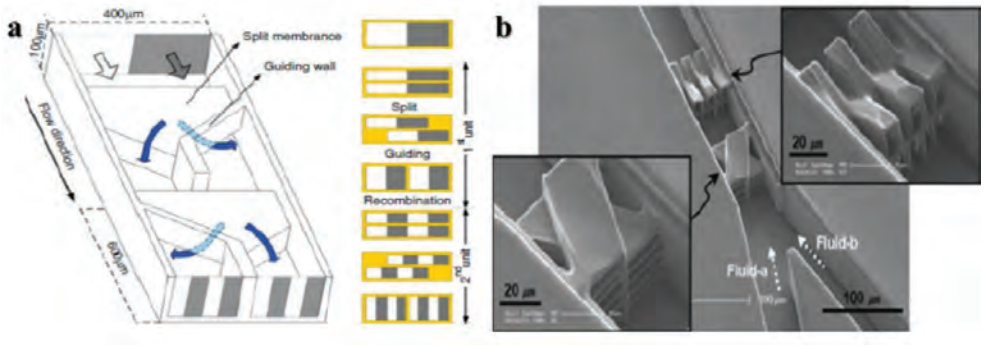

Figure 4 (a) Split and recombine micromixer main channel [27], (b) complicated geometries built inside of SAR micromixer [28].

The main disadvantage of Parallel lamination and SAR micromixers is the complex fabrication of the 3D structure. However, an effect similar to the split and recombine can be done within a planar microfluidic using Dean vortices as shown in Figure 5. Dean flows occure when fluid travels through a curvilinear channel, where it experiences an interplay between inertial force acting to axial motion and centrifugal force acting along the channel's radius of curvature. "These effects produce a radial

pressure gradient whose magnitude is sufficient to generate a transverse flow field" [29].

2.1.4 Focusing enhancement. An easy solution to reduce the mixing path is focusing of the mixing streams. Focusing can be either geometrically [31] or hydrodynamically. Geometrical focusing decreases the width along the microchannel gradually, to enhance mixing by achieving thinner streams and smaller lamination width (Figure 6a)." Mixing time is inversely proportional to the square of the diffusion path length (in this case represented by the focused stream width)" [26], therefore, a decrease in the stream width will result in faster mixing. The same thing is applicable for the hydrodynamic focusing, however in this case the sample flow of solute and solvent will be already flowing in parallel lamination, and a sheath flow of different phase will be induced in both direction to decrease the width of that stream (Figure 6b).

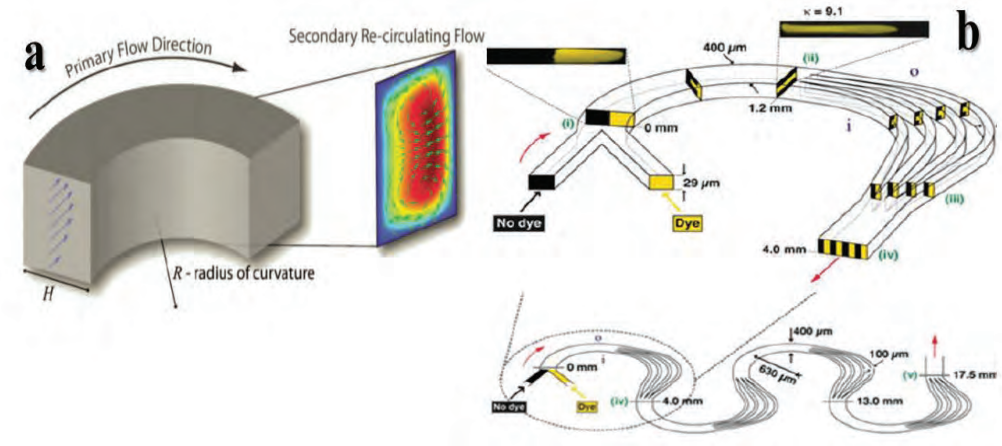

Figure 5 (a) Curved unit of the split and recombine micromixing channel and its corresponding cross-section view of the flow [29]. (b) Three-dimensionally micromixer, named crossing manifold micromixer [30].

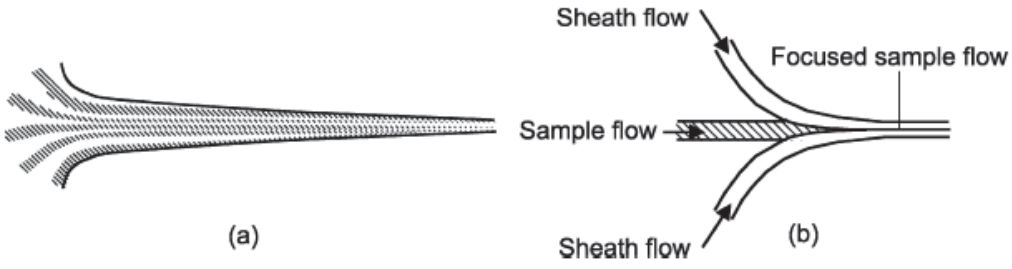

Figure 6 Focusing concepts: (a) geometric focusing, (b) hydrodynamic focusing [26].

2.1.5 Chaotic advection micromixers. Advection usually describes the transport of a substance within a moving fluid. It usually happens in the direction of the flow, which means that it has no effect on the transversal component of the flowing fluid. However, if there are advections that occur in other directions, so-called chaotic advection [32], can generate transverse components of flow [33]. The different types of chaotic advection can be done by stretching, folding and breakup processes. It can occur by active external disturbances or passively by spatially periodic structures inside the channel itself. When the flow passes through these structures (also referred to as advection cycle), these structure manipulate the initial flow direction, and the streamlines create vortex type flow and recirculation that create the transversal mass transport. By repeating these advection cycles of stretching, folding and breaking up the fluids leads to a complete mixing. The obstacles can be inserted in the walls of the microchannel [34] or into the channel itself [35, 36]. Inducing different structures are only effective at high Reynolds numbers (Re > 100) [35]. However, recently reported micromixers with optimized cubic and rectangular structure capable of mixing with Re < 1 [36, 37] as shown in Figure 7. Also, a combination of SAR with chaotic advection micromixers have been presented [38-41].

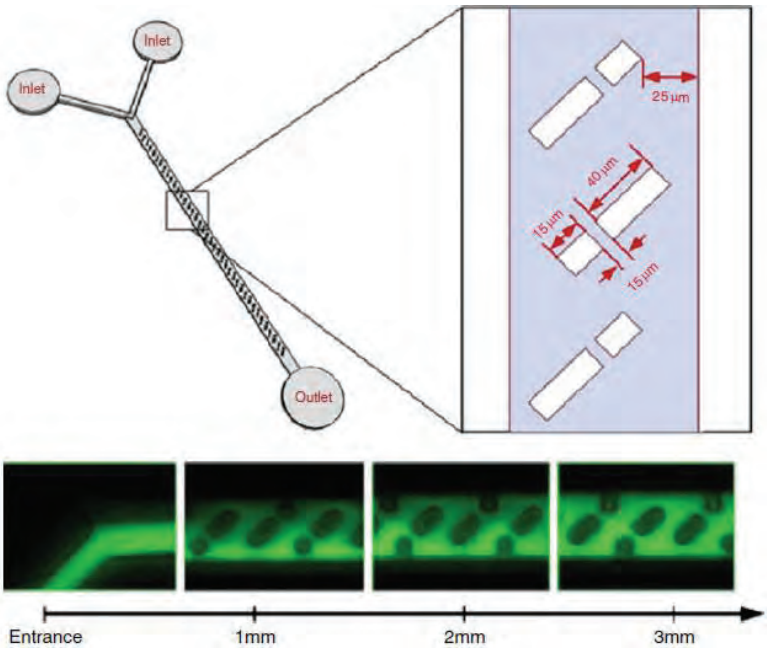

Figure 7 Mixing with rectangular structure with key features and dimension. Mixing is occurring at Re = 0.051 [36, 37].

2.1.6 Multiphase and microdroplet-based micromixers. Introduction of microdroplets inside the microchannel enhances mixing of the merged streams due to the internal circulation formed inside the droplets and in the sheath flow surrounding the droplets. Microdroplets can be generated within microchannels by using different methods such as micro injectors, needles, and electric fields [42-44]. However, flow instabilities between immiscible fluids is the most used method for droplet generation.

The basic configuration of a droplet generator is shown in Figure 8 for the T-junction and flow focusing. In the T-junction configuration, the channel transporting the solute and solvent intersects perpendicularly with the continuous oil channel, and at their intersection a droplet is formed. By varying the flow rates, channel dimension, or viscosity of the two phases, the dimensions of the microdroplet can be controlled [45, 46]. In flow focusing configuration, the solvent and solute flow in two lateral channels, whereas the carrying fluid flows in the middle [47].

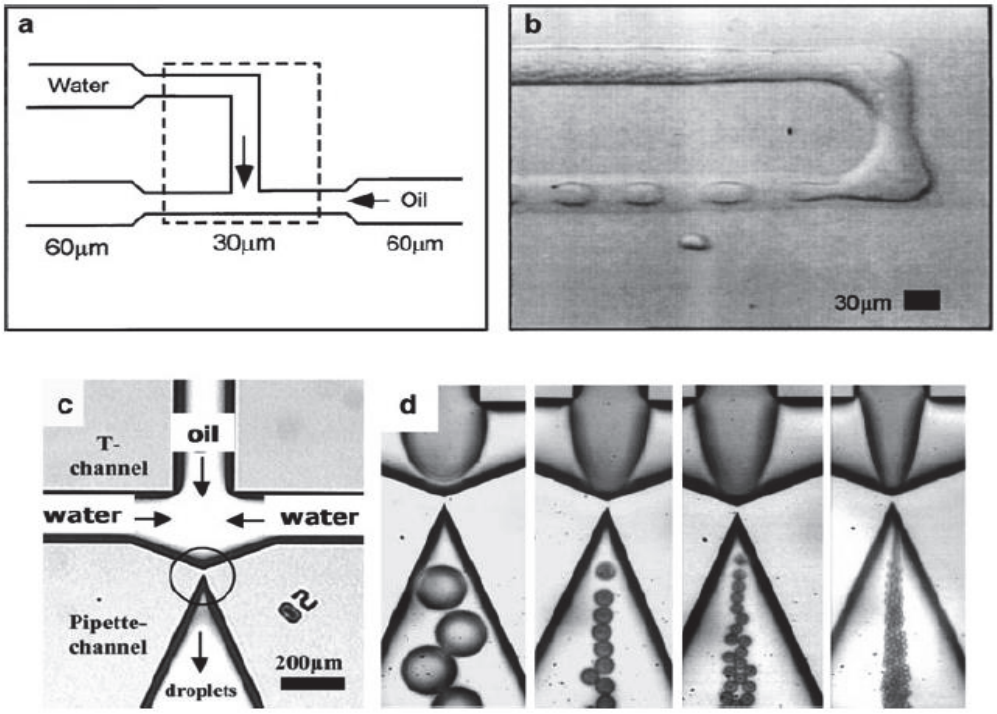

Figure 8 Droplet formation in the microdroplet micromixer (a) T-junction to create droplet and (b) photo of water in oil formation [45], (c, d) Flow focusing configuration [47].

Geometrical confinement inside the droplets brings the two solutions close to each other and reduces the diffusion length, which results in enhanced mixing. Furthermore, the contact of the microchannel walls and the droplet surfaces causes the generation of recirculating flow inside of the droplet itself [48] (Figure 9a). When the droplet is moving through a straight channel, the recirculation flows are generated evenly in the upper and lower part the channel. Each recirculation pattern consists of counter circulating flows. This flow pattern provides a mixing in the two parts. However, mass transport is not achieved, since they remain separated and unmixed [48]. To create the chaotic advection within the microdroplet, the channel geometry must vary to create stretching and folding process inside of the liquid droplet [49] as in Figure 9b.

An easy way to induce chaotic advection is by introducing turns or bends in the channel to create unequal recirculating flow in the upper and lower part of the droplet [49-51]. This type of micromixer is also called planar serpentine micromixer (PSM).

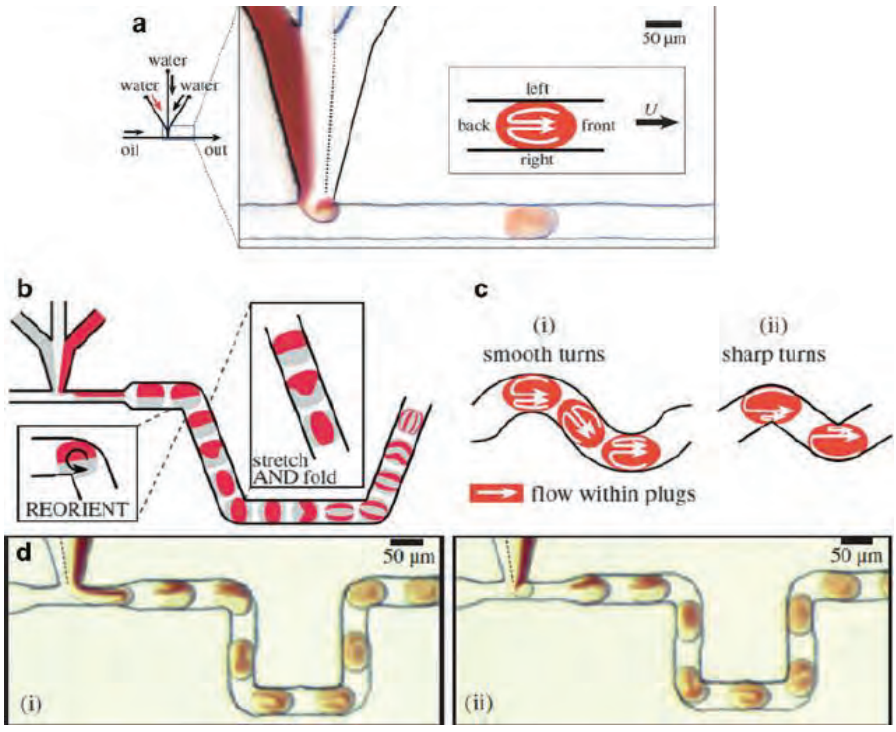

Figure 9 Mixing of microdroplets: (a) Recirculation flow generation, (b) mixing pattern that stretches, folds and rotates the fluids interface, (c) asymmetrical recirculation inside of droplets, and (d) Chaotic advection inside of a micro droplets [51].

When the droplet moves through the channel each part is in contact with different section of the turn. The half that is exposed to the inner arc is in contact with a shorter section, while the other is in contact with the larger section of the outer arc. Within the part that is exposed to the inner section, a smaller recirculating flow is generated compared with the opposite part. This distribution of flow with the alternate switching of the streams causes a chaotic and crossing streams as shown in Figure 9c.

Another multiphase technique introduces a gas bubble into the laminated flow stream to create a circulation inside of the flow, it consists of liquid plugs separated by inert gas bubble [52]. Figure 10 shows the circulation in the fluid filling the microchannel between the gas droplets.

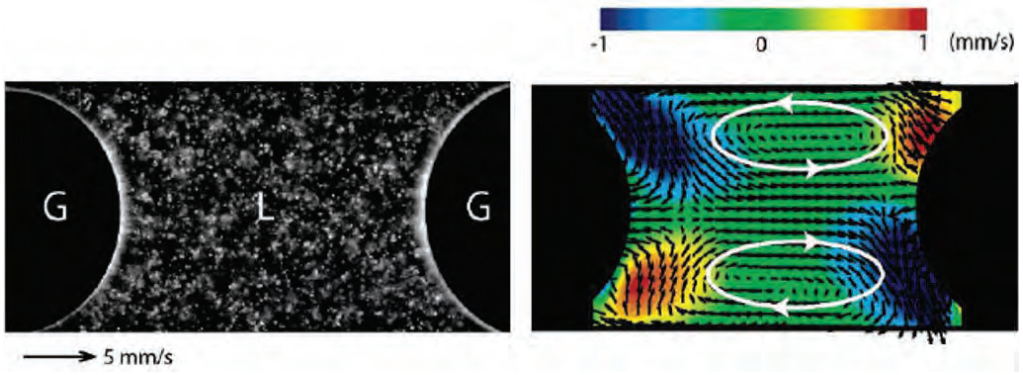

Figure 10 Circulation in the fluid between the gas droplets inside of the microchannel, digital image (left) and the vector field with a spanwise velocity component as a color contour (right) [41].

2.2 Active Micromixers

2.2.1 Sequential segmentation. In sequential segmentation the solvent and solute streams are broken up axially along the mixing channels, each segment occupies the entire width of the channel. The parabolic velocity profile results in axial dispersion several orders of magnitude compared to pure molecular diffusion according to Taylor-Aris dispersions in equations (5-7) [53].

Sequential segmentation concept uses alternative switching of the inlet flows (Figure 11). The mixing ratio, can be adjusted by the switching ratio of the inlets.

There are few studies that used sequential segmentation in enhancement of mixing using Taylor-Aris dispersion [53-62]. Segmentation of the flow can be done

using piezoelectric valves to control highly pressurized fluids [60], or piezoelectric actuators to initiate the flow [53, 60, 62].

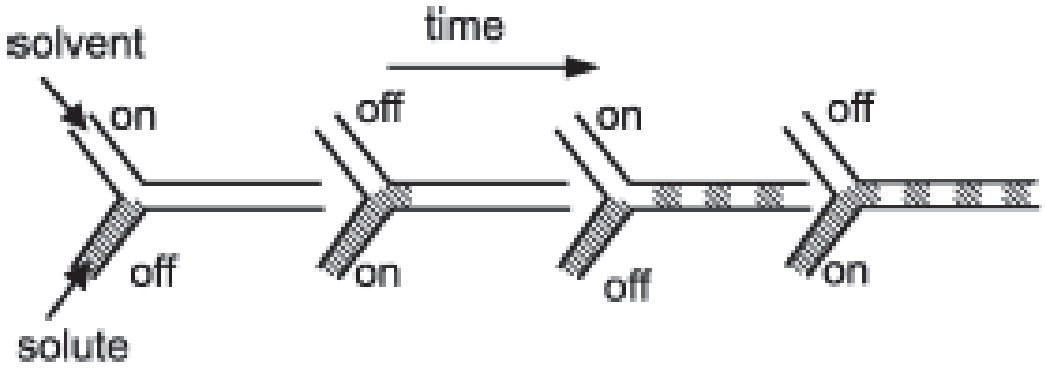

Figure 11 Sequential segmentation: alternative switching of the inlet streams [53].

Further improvement was done by coupling hydrodynamic focusing with sequential segmentation to get rid of the side effect of Taylor-Aris dispersion in a rectangular microchannel [61]. Sequential segmentation mixing flow with obstacles is reported in [63]. A computational study of a pulsing velocity fluid that is switching the flow rate in the inlet channel periodically from high to low has been presented [57], and is shown in Figure 12.

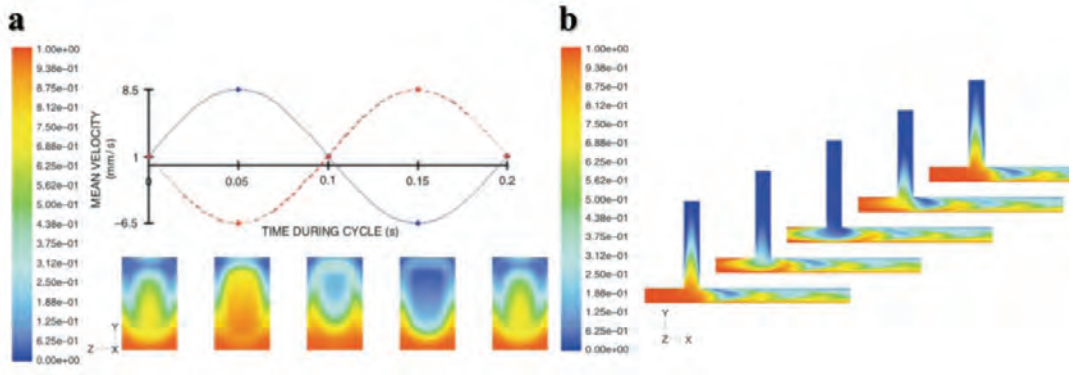

Figure 12 Mixing by sequential segmentation for a perpendicular inlet channels. (a) Contour levels of the different solutions mass fraction in Y, Z plane. (b) Contour levels in the Y, X plane [57].

The latest work done in this area to further decrease the mixing path and time, is done using 3 inlets with forward and reverse flows that are controlled by a fast switching micropump with a frequency of 400 Hz [59]. As a proof of the efficiency of sequential segmentation in mixing improvement, it was used to synthesize gold nanoparticles with high uniformity [58].

2.2.2 Thermal disturbance. Natural convection can be also used to enhance mixing on the microscale. For example, it was used in conjunction with thermal disturbance to perform a polymerase chain reaction (PCR) with a pumpless micromixer [64]. Moreover, according to equation 2, the diffusion coefficient increases with increasing the temperature. Therefore, thermal energy can be used as a mixing enhancer in microchannels [65, 66].

2.2.3 Electrokinetic disturbance. Elecrokinetic instability (EKI) (or disturbance) micro mixers (Figure 13a), is when electric field fluctuates and induce mixing in microfluidic channels [67, 68]. This fluctuating electric fields causes stretching and folding of the fluid boundaries that mixes the fluid stream in highly laminar flow (Re < 1).

An electrically charged heterogeneities is introduced to enhance mixing efficiencies by creating localized regions of flow circulations [69], the results are illustrated in Figure 13b.

2.2.4 Dielectrophoretic disturbance. Dielectrophoresis is a phenomenon by which polarization of a particle is induced by a non-uniform electric field. The polarized particles moves to and from the electrodes in response to the electrical field applied to it. The creation of chaotic advection is caused due to the joint effect of the movement of the particles and the geometry of the channel [70-72]. A proved experiment shows that mixing a small sample volume can be done in a controllable manner to trigger a reasonably quick mixture. This sort of mixer does not need complex geometry and can be helpful in the field of digital microfluidics [72].

2.2.5 Magneto-hydrodynamic disturbance (MHD). MHD relies on the induction of Lorentz body forces in an electrolyte solution. MHD mixers utilize an array of electrodes placed within the channel walls to create current flows that allows the

fluid to be mixed with the presence of alternate potential difference on the electrode pair [73-75]. Lorentz body force normally happens while coupling the generated electric field and magnetic field couples as described in Figure 14.

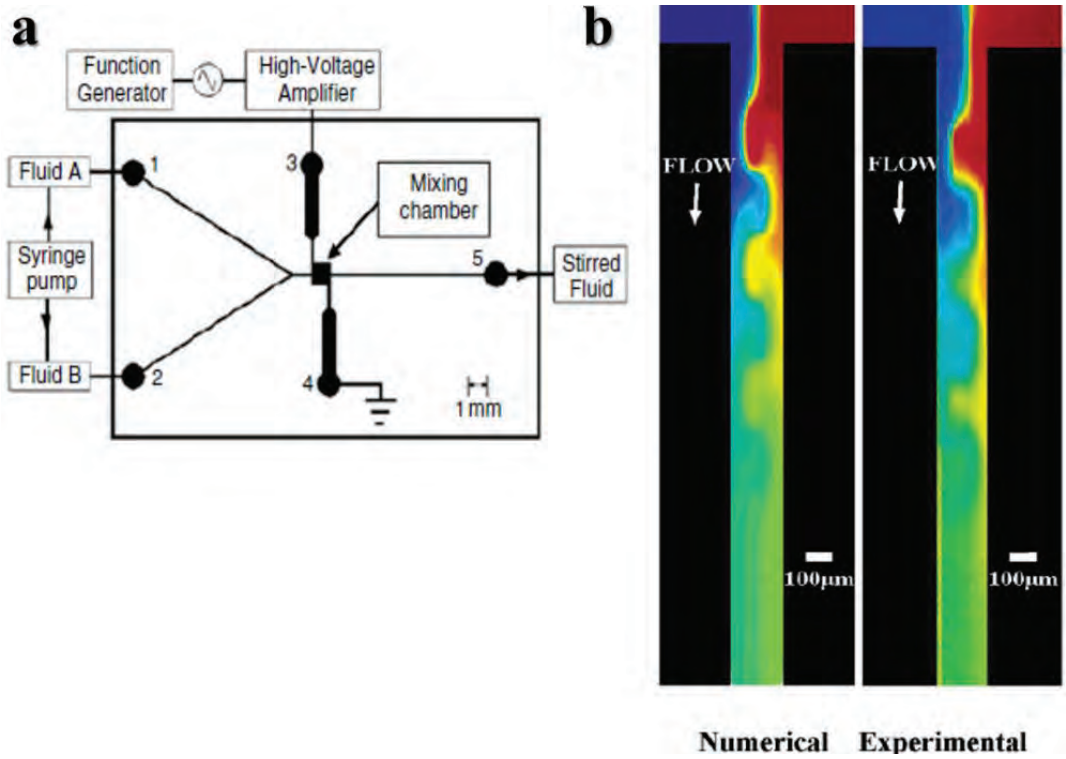

Figure 13 (a) Electrokinetic micromixer. Fluids are pumped from both inlets and passes through the AC excitation mixing chamber [67]. (b) Mixing chamber with heterogeneous staggered patches of different zeta potential [69].

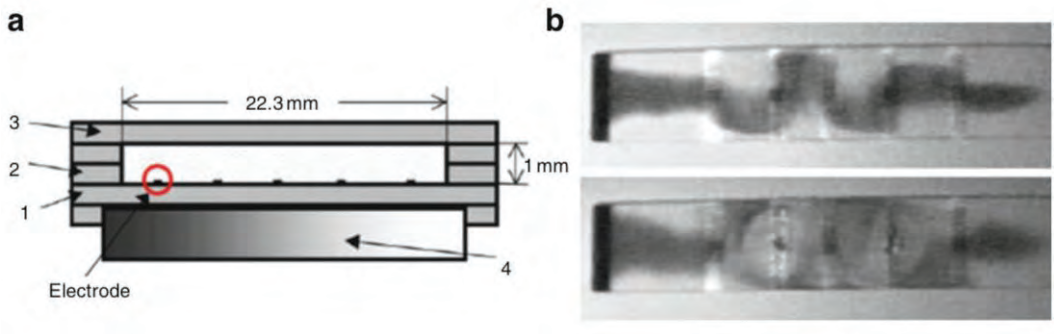

Figure 14 Magneto-hydrodynamic micromixer. (a) Cross-section view of the mixer. (b) Fluid deformation across the channel [73].

2.2.6 Acoustic disturbance. Mixing using acoustic waves can be used in micromixers to locally shake fluids involved. Piezoceramic/silicon transducers are used to generate acoustic streaming flow [76, 77]. The ultrasound disturbance causes an acoustic whirl type of mixing on the fluid perpendicular to the flow direction, which leads to a good turbulent-like mixing at Re < 1 inside of the microchannel [76] or chamber [77, 78].

Air bubbles are also used in an acoustic micromixer in order to enhance mixing. Exposing the surface of an air bubble inside of a liquid medium to a sound field allows it to act as a vibrating membrane. This vibration causes a bulk fluid movement around the air–liquid interface. This technique, which is called cavitation microstreaming can be implemented using a single bubble as shown in Figure 15 [79] or using an array of bubbles [80, 81].

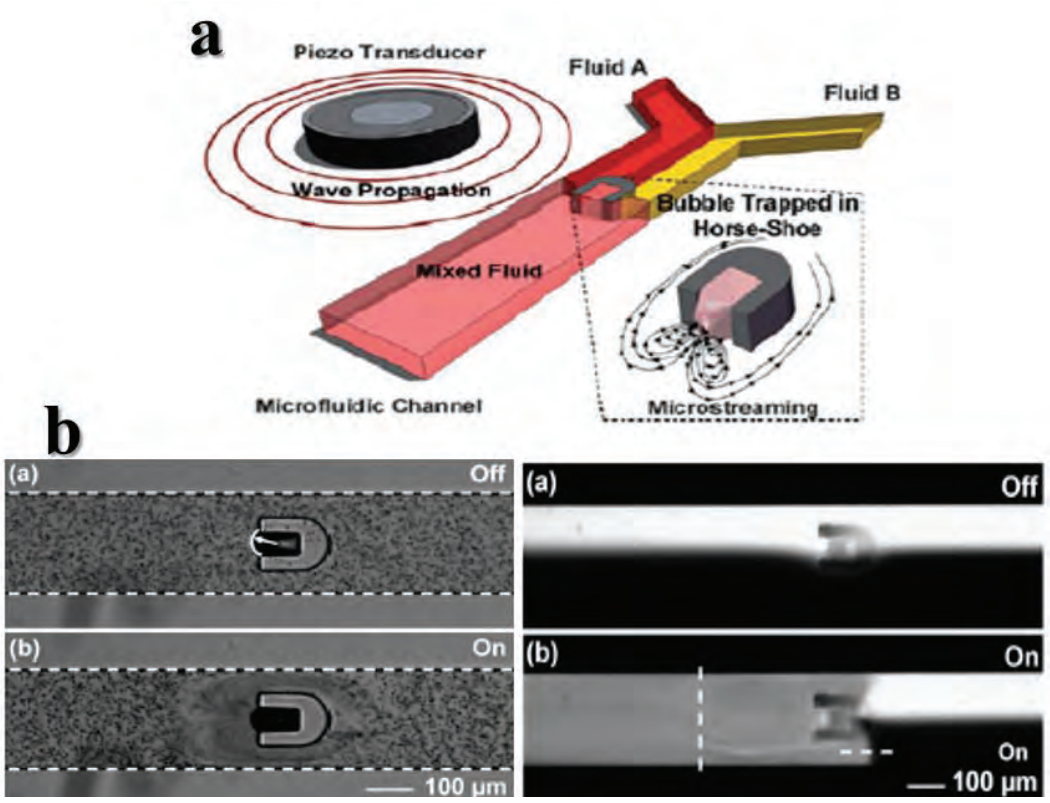

Figure 15 Acoustic micromixer. (a) Micromixer configuration with all of its components, an air bubble inserted within the channel to generate a vibrating motion that mixes the two solutions. (b) Photomicrographs showing streams and concentration while the acoustic waves are switched off and on [79].

2.3 Objectives

The objectives of this thesis is to model improvement of mixing inside a microchannel using sequential segmentation of fluid streams. Sequential segmentation has the potential to increase species dispersion by three orders of magnitude [12]. However, until now, it has been only studied in 2D (slit microchannel) which is not enough to guide design optimization of such micromixers. To gain a better understanding of the different parameters that affect mixing efficiency in sequential segmentation, a finite-element model of mixing inside different microchannel shapes will be built using COMSOL Multiphysics to study the effect of the following parameters:

1. Frequency of segmentation (how fast the liquid streams are switched on and off).
2. Flow velocity.
3. Duty cycle (DC) of the segmentation (duration of the solvent pulse relevant to duration of the anti-solvent pulse).
4. Shape of microchannel cross section (rectangular, triangular, circular).
5. Aspect ratio of the microchannel (Height/Width)
6. Flow configuration and branches (Y-shaped, T-shaped, Arrow head shape, and Hydrodynamic focusing).

Chapter 3. Numerical Analysis Using COMSOL Multiphysics

COMSOL Multiphysics was used to study mixing improvement by sequential segmentation of liquid streams. COMSOL is a commercial package used for modeling and simulating physics-based problems numerically based on Finite Element Method (FEM). FEM is an advanced numerical technique used for solving boundary value problems that can be described by partial differential equations (PDEs). COMSOL has a user friendly interface that lets the user build and simulate physical problems through a systematic procedure.

Laminar Flow and Transport of Diluted Species modules were used to simulate sequential segmentation phenomenon for a three dimensional geometry with time dependence. The selected modules are interdependent as the velocity field obtained by the laminar flow module is used to calculate mass transfer of the solute using the transport of diluted species module.

3.1 Modeled Geometries

Different microchannel geometries have been simulated and classified according to the following criteria:

1. Inlet flow configuration (Y-shape, T-shape, arrow-head, and hydrodynamic focusing).
2. Microchannel cross section (rectangular, triangular, circular).
3. Microchannel aspect ratio (4:1, 1:1, 1:4).

A sketch of each geometry with all different cross-sectional areas is shown in Figure 16.

3.2 Governing Equations

3.2.1 Laminar flow. A three-dimensional transient incompressible laminar flow with constant properties model was selected to solve the continuity equation, Eq. 13, and the conservation of momentum equation, Eq. 14, to obtain the flow field and pressure distribution throughout the microchannel.

Continuity:
$$\frac{D\rho}{Dt} = -\rho\nabla \cdot \mathbf{v} \tag{13}$$

Momentum:
$$\rho\frac{D\mathbf{v}}{Dt} = -\nabla p - [\nabla \cdot \boldsymbol{\tau}] + \rho\boldsymbol{g} \tag{14}$$

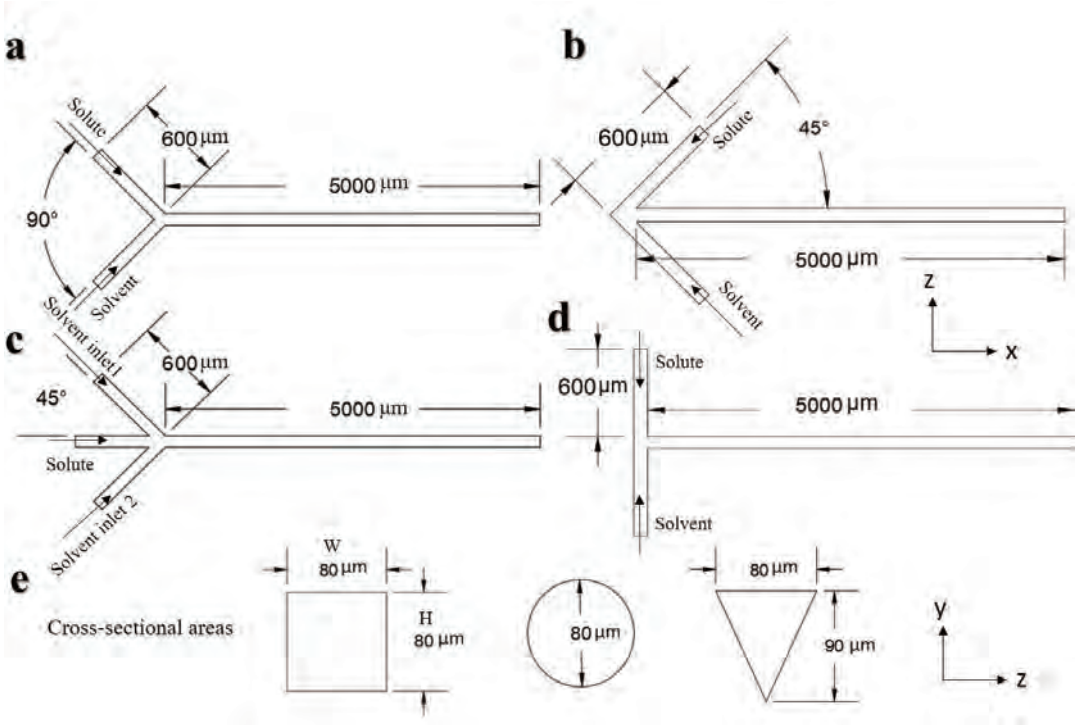

Figure 16 Geometry of microchannels and their different cross-sectional areas. (a) Y-shaped micromixer (b) arrow head shaped micromixer (c) three inlet micromixer (hydrodynamic focusing) (d) T-shaped micromixer. (e) Different microchannel cross-sectional shapes were studied including rectangular, circular and triangular. W indicates the width and H is the height of the microchannel.

where ρ is density, p is pressure, $\boldsymbol{g}$ is the gravitational acceleration term (neglected in the present simulation), $\mathbf{v}$ represents the velocity vector in three-dimensions. $\boldsymbol{\tau}$ The viscous stress tensor, is given by $\boldsymbol{\tau} = -\mu(\nabla\mathbf{v} + (\nabla\mathbf{v})^T)$, where $\nabla\mathbf{v}$ is the velocity gradient tensor of components $\frac{\partial v_j}{\partial x_i}$, $(\nabla\mathbf{v})^T$ is the transpose of the velocity gradient tensor with components $\frac{\partial v_i}{\partial x_j}$, μ is viscosity, and $(\nabla \cdot \mathbf{v})$ is the divergence of the velocity vector. Fluid properties such as density, viscosity, and diffusion coefficient were assumed to be independent of liquid pressure.

3.2.2 Transport of diluted species. The equation of continuity for a multicomponent mixture. (Assuming dilute liquid solutions and constant temperature and pressure) is described by Eq. 15.

$$\rho\frac{D\omega_\alpha}{Dt} = -(\nabla \cdot \mathbf{j}_\alpha) + r_\alpha\,, \qquad (\alpha = 1,2,\cdots,N) \tag{15}$$

where $\omega_\alpha = \rho_\alpha / \rho$ is the mass fraction of species α, $\mathbf{j}_\alpha = -\rho D \nabla \omega_\alpha$ is the mass flux of species α, and r_α is the rate of generation per unit volume. (The component of the convection term are taken from the momentum solutions and the reaction term is neglected).

3.3 Boundary Conditions and Properties

3.3.1 Laminar flow. All cases have a no-slip boundary condition at the walls of the microchannel, an outlet pressure of 1 atm, and constant properties of $\mu = 10^{-3}$ Pa·s and $\rho = 1000$ kg/m^3. The inlet boundary conditions in the laminar flow module were varied in the different cases to simulate flow segmentation as described in Table 1. Nevertheless, regardless of the segmentation profile, the velocity at the inlet was set as fully developed. The wave functions listed in Table 1 were used for inlet fluid flow conditions to produce pulsating flow. Wave function on all inlets were synchronized to produce the segmented flow as desired.

For a square wave function, amplitude, duty cycle and frequencies are directly specified for each separate case in the wave function settings, which is shown for the 50% DC with 150 Hz case in Figure 17. While specifying the wave function as inlet boundary condition, it is required to add a vertical shift of (+0.005) to produce an on-off switching wave of amplitude 10 mm/s, and phase shifts of (π/frequency) to construct the synchronization between the pulses.

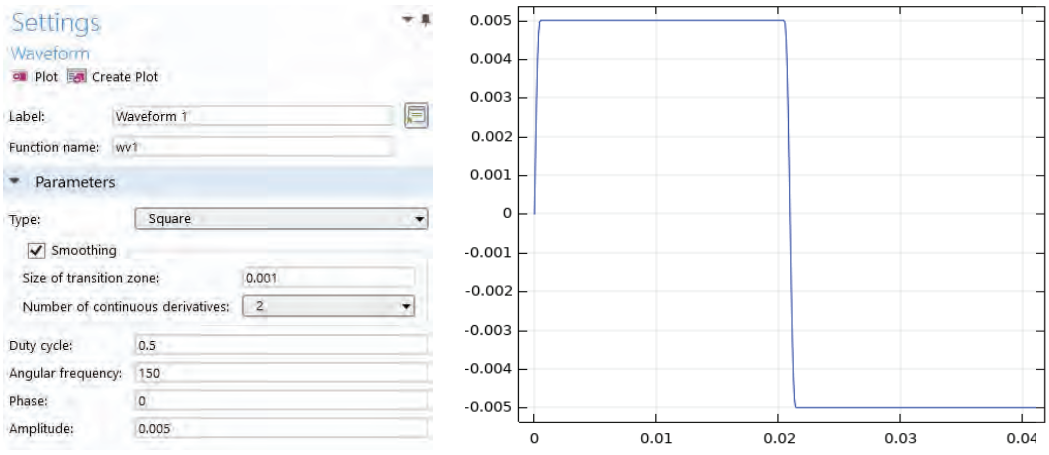

Figure 17 Square wave function settings for 50% Duty cycle, 150 Hz and 5 mm/s.

3.3.2 Transport of diluted species. Boundary conditions for transport of diluted species are straight forward. The inlet concentration of the pure solvent stream was set as 0 mol/m^3, the inlet concentration of the solute was set as 1 mol/m^3, and the initial concentration in the entire channel was set as 0 mol/m^3.

Table 1: Laminar flow fully developed average velocity inlet boundary conditions for different cases, units in mm/s.

Case	Solute	Solvent
No Segmentation	10	10
50% DC with 50 Hz, 2 inlets	10*square(t)	10*square(t+(pi/50))
50% DC with 100 Hz, 2 inlets	10*square(t)	10*square(t+(pi/100))
50% DC with 150 Hz, 2 inlets	10*square(t)	10*square(t+(pi/150))
50% DC with 200 Hz, 2 inlets	10*square(t)	10*square(t+(pi/200))
25% DC with 150 Hz, 2 inlets	10*square(t)	10*square(t+(pi/100))
75% DC with 150 Hz, 2 inlets	10*square(t)	10*square(t+(pi/300))
50% DC with 150 Hz, 3 inlets	10*square(t+(pi/300))	In1: 10*square(t) In2: 10*square(t+(pi/150))

3.4 Solver

COMSOL categorizes solvers available to solve the set of partial differential equations involved as direct or iterative solvers. Each category has its advantages and disadvantages. In general, direct solvers are faster and more accurate than the iterative ones but need high machine capabilities (especially the number of cores and RAM size)

otherwise it runs out of memory. This is particularly challenging for three dimensional models or nonlinear geometry models.

The direct solvers used by COMSOL are the PARDISO, MUMPS and SPOOLES solvers. All of the solvers are based on LU decomposition. These solvers will all arrive at the same answer for all well-conditioned finite element problems, which is their biggest advantage, and can even solve some ill conditioned problems. From the point of view of the solution, it is irrelevant which one of the direct solvers is chosen, as they will provide the same solution. The direct solvers differ primarily in their relative speed. The MUMPS, PARDISO, and SPOOLES solvers can each take advantage of all of the processor cores on a single machine, but PARDISO and MUMPs tend to be faster than SPOOLES.

SPOOLES also tends to use the least memory of all of the direct solvers. All of the direct solvers do require a lot of RAM, but MUMPS and PARDISO can store the solution out-of-core, which means that they can offload some of the problems onto the hard disk. The MUMPS solver also supports cluster computing, which allows the use of more memory than is typically available on a single machine.

The iterative methods approach the solution gradually, rather than in one large computational step as in the direct solver. A tolerance should be chosen for the iterative solver, a tighter tolerance produces a greater accuracy on the available mesh, or a looser tolerance for a faster solutions. It is more reasonable to refine the mesh rather than tightening the tolerance, since tighter tolerance is solved on the used mesh. The big advantage of the iterative solvers is their memory usage, which is significantly less than a direct solver for the same sized problems. The big disadvantage of the iterative solvers is that they do not always work, and the accuracy of the results usually depends on tolerance and mesh size, whereas the direct solver only depends on the mesh size, since the tolerance is automatically changes during the iterations. In our case the direct solver with MUMPS is used.

3.5 Mesh

3.5.1 Mesh details. A mesh of 760 thousand elements was used in this study, Figure 18. Mesh parameters were set manually to refine mesh size in areas of highest gradients. The functions used in COMSOL in this regard were corner refinement, free tetrahedral elements, and boundary layer techniques. The specified values for each technique are illustrated in Figure 19.

3.5.2 Mesh dependence. After defining all the boundaries of the microchannel device, the finite element mesh is created. The model is firstly checked to be mesh independent with a good mesh quality. In order to make sure that the study is mesh independent, the concentration distribution over the microchannel cross section was plotted for different mesh sizes to assess the mesh independence of the obtained solution. Calculation were conducted across the microchannel at a cross section 2 mm downstream of the inlet junction. The mesh was refined until the change in concentration profile became negligible with the increase in the number of mesh elements. As shown in Figure 20, the calculated concentration across the microchannel cross-section becomes independent of mesh size at 760,000 elements.

To avoid severe irregularities in element shape which may cause inaccurate results, Mesh Quality Test (MQT) was conducted and a reasonable average mesh quality (more than 0.65) was confirmed over the whole geometry as shown in Figure 21.

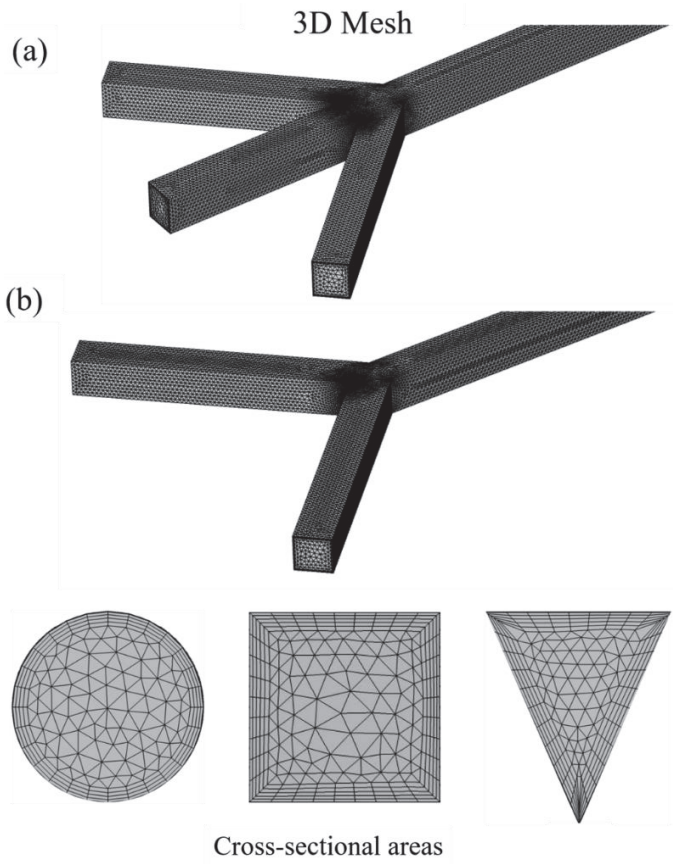

Figure 18 3D and cross-sectional mesh, (a) hydrodynamic focusing microchannel, (b) Y-shaped microchannel.

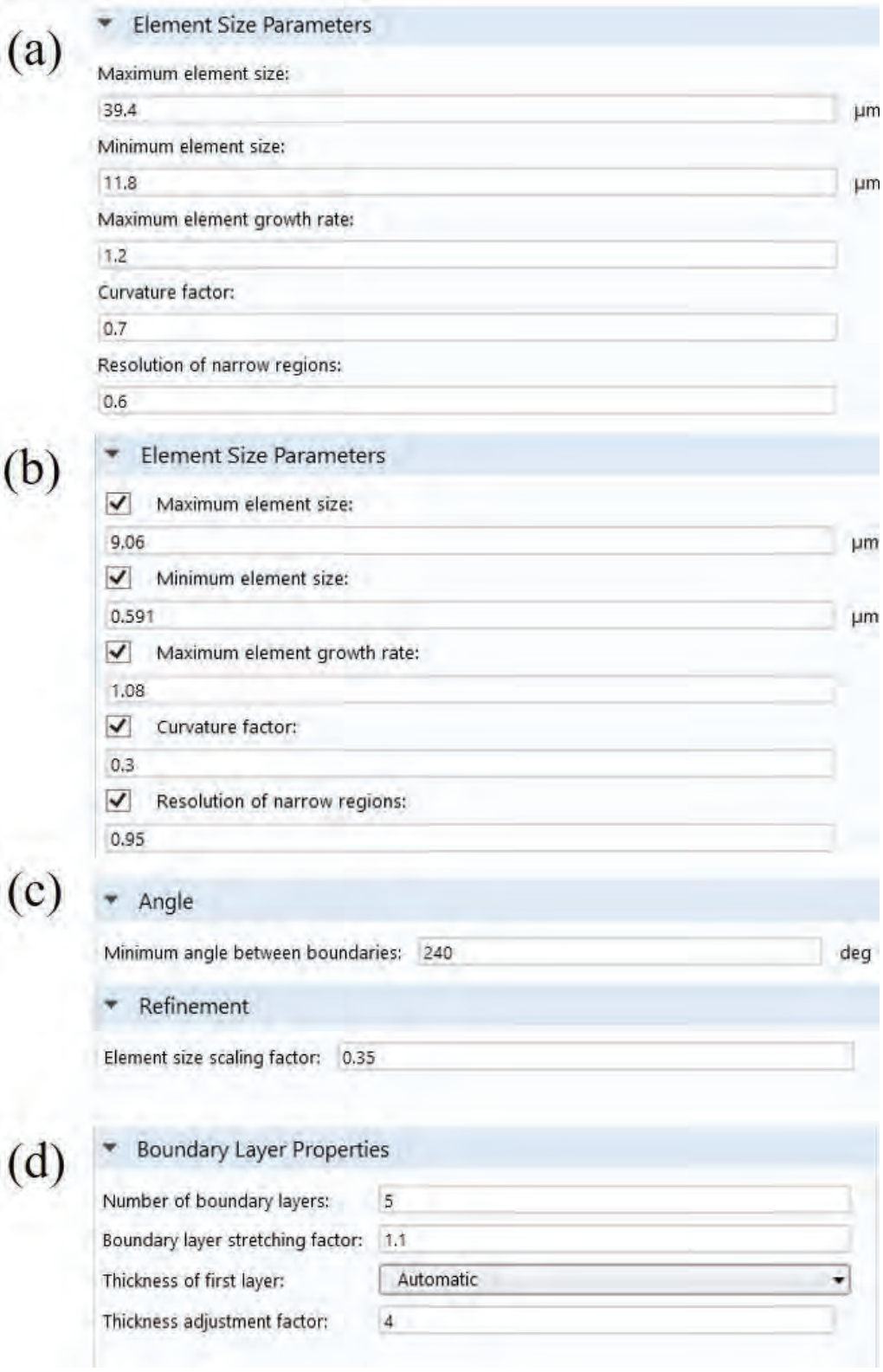

Figure 19 Used meshing techniques and their specific values. (a) Inner mesh size, (b) outer boundary size1, (c) corner refinement, (d) boundary layer property.

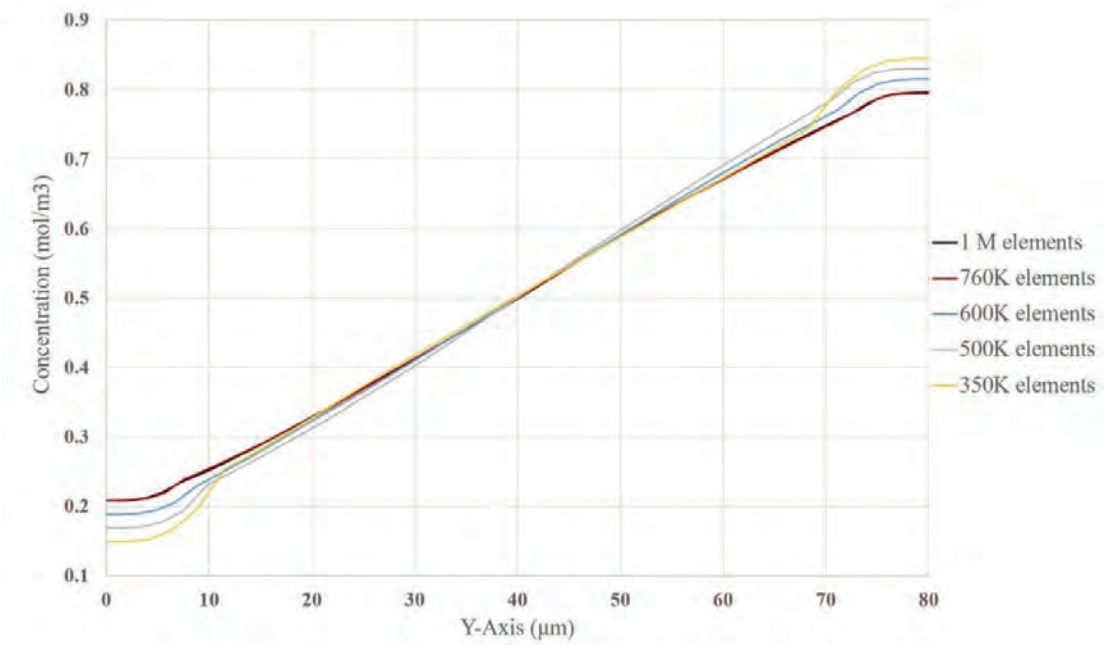

Figure 20 Mesh independent test for the concentration across the microchannel in the mid-plane.

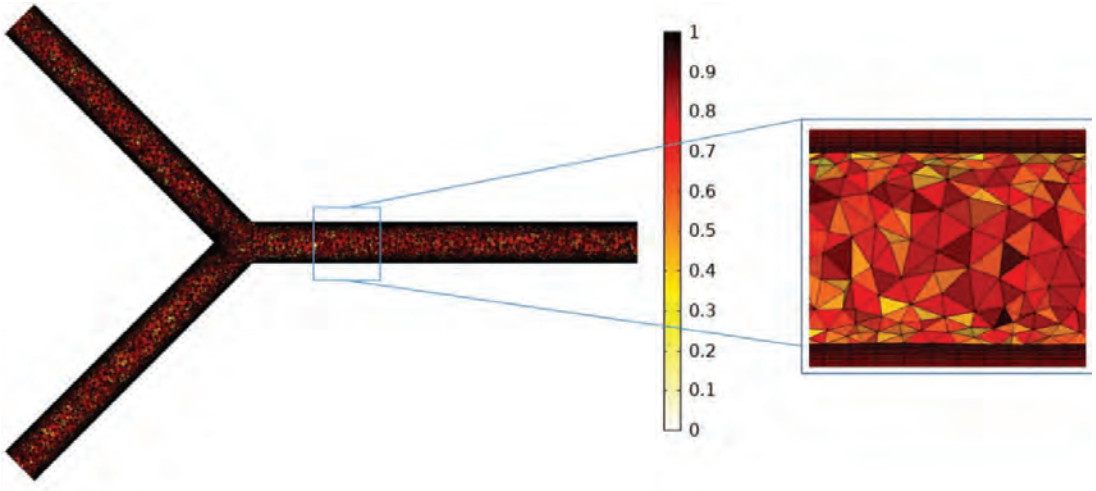

Figure 21 Mesh quality test, on the right side a zoomed segment is taken to show the boundary layer and inner tetrahedral mesh qualities.

3.6 Computational Time

The total simulated time of this study was 0.95 seconds. Time step size was controlled by the direct solver and it is changed automatically through the iterations to

produce an accurate solution. The tolerance is set to be 10^{-5}. The average computation time per case is 70 hours on a 12-core Intel Xeon gold 5118 processor with 48 GB of RAM.

3.7 Model Validation

To confirm accuracy of our COMSOL model, we had to validate our model by reproducing data in a relevant previous study. After survey of the literature, the most suitable results to reproduce were found in a study by Mengeaud et al. [82]. In this study, a zigzag microchannel was used to enhance mixing of two liquid streams, Figure 22. The microchannel features two perpendicular feeders 100 μm wide (*w*) each that merge into a zigzag channel having the same width 90° turns. The pitch of the zigzag pattern was defined as a variable periodic step (*s*). The linear length of the zigzag channel (*L*) is fixed to 2 mm. The mixing efficiency in this paper is quantified by the ratio c_{min}/c_{max} between the minimum and the maximum concentrations at the outlet cross section. All of the validated cases were done with a very fine mesh. Figure 23 shows the constructed mesh with a zoomed in segment around the junction on the bottom side. Figure 24 shows the concentration profile for the four geometrical cases.

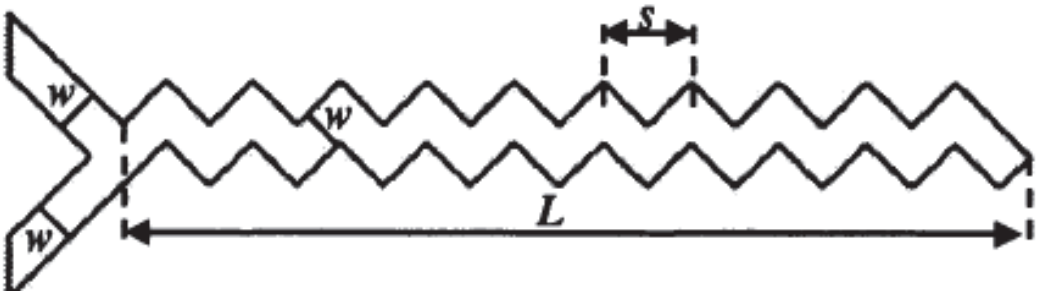

Figure 22 Dimensions of the microchannel that is used for validation, with *w* as the width of the channel; *s* as the linear length of the periodic step; and L, the linear length of the zigzag microchannel [82].

The validation was conducted by studying the effect of the geometry ratio (*s*/*w)* on the mixing efficiency at Pe = 2600 and Re = 267 as portrayed in Figure 24. As can be seen from Figure 24, the COMSOL model was able to reproduce the results in [82] with a maximum deviation of 7% and around 2% in most of the studied range of (s/*w).* This data implies that COMSOL Multiphysics model is able to predict the concentration behavior throughout complicated microchannel geometries.

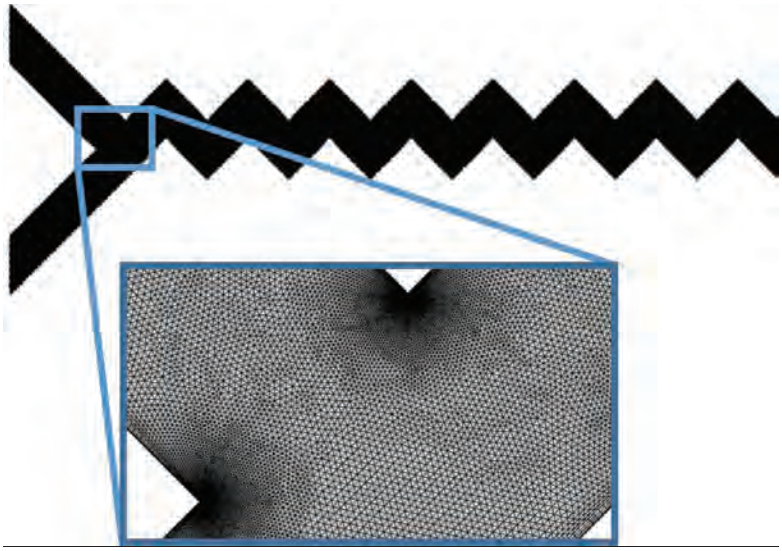

Figure 23 Mesh of the validated microchannel with (s/w) = 1, on the bottom side a zoomed segment is taken to show the fine mesh.

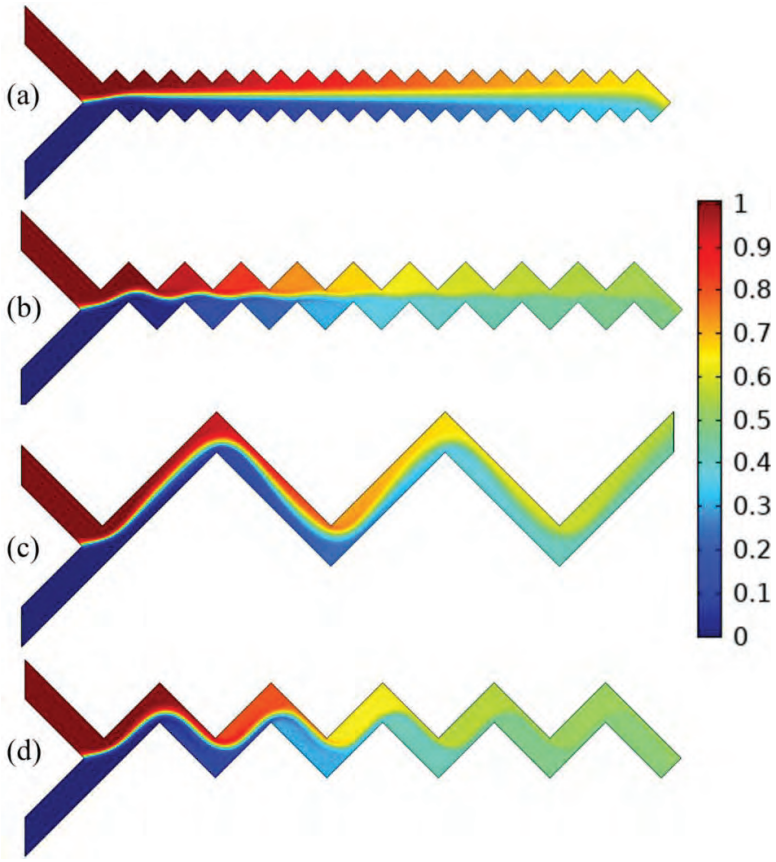

Figure 24 Concentration profile alone the zigzag microchannel, (a) (s/w) = 1, (b) (s/w) = 2, (c) (s/w) = 4, and (d) (s/w) = 8, solute concentration is equal to 1 (red) and the solvents concentration is equal to 0 (dark blue).

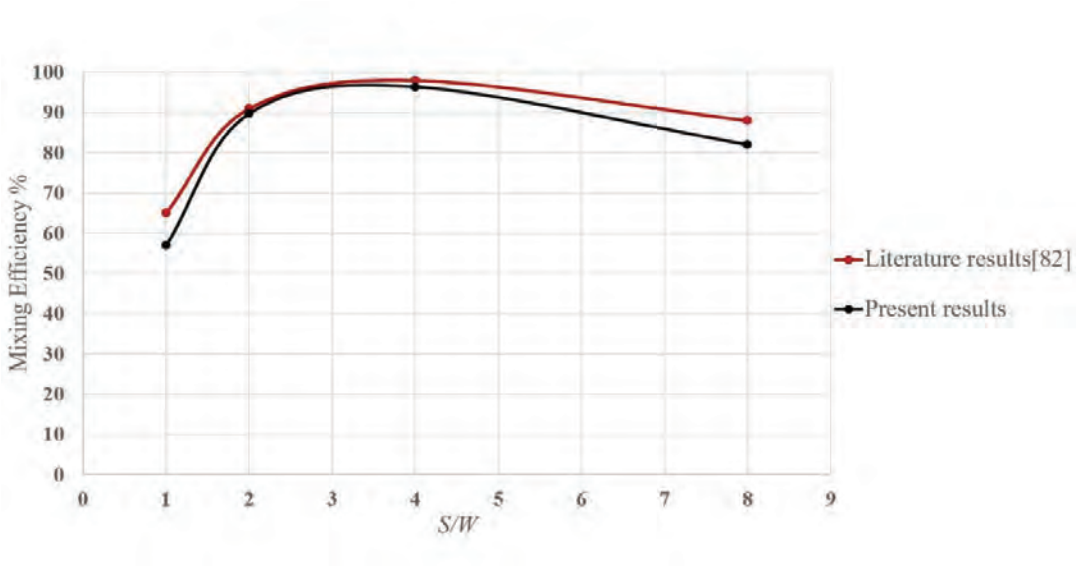

Figure 25 Effect of the geometry ratio *s*/*w* on the mixing efficiency at Pe = 2600 and Re = 267. Red line represents the literature data, while the black line represents COMSOL Multiphysics simulation results.

Chapter 4. Results

In sequential segmentation, two solutions (solvent and solute) are alternately pumped into a mixing microchannel by switching the flow in each inlet branch on and off alternatively. This is usually achieved by applying pressure to both inlets and using solenoid valves to switch flow in each branch on and off. Subsequently, discrete plugs from the two solutions are introduced into the microchannel and diffuse through the microchannel. This is an efficient method for mixing solutions, because it is capable of reducing the mixing time by changing the switching frequency of pumping for decreasing the diffusion length of alternate layers of the two solutions. In order to achieve more rapid mixing, switching frequency should be increased according to the literature.

The principle of sequential segmentation for a Y-shaped microchannel with two inlets and a three-inlet microchannel is shown in Figure 26. In this method both solvent and solute are alternately pumped into the mixing channel to produce alternate layers of the two solutions. The two solutions subsequently inter diffuse through their interface in the mixing channel. The segment thickness is determined by the flow rate and switching frequency of pumping of the two solutions. The decrease in segment thickness leads to an increase in mixing speed, since the diffusion time necessary to mix the two solutions is proportional to the square of the segment layer thickness [59]. Using this mixing method, mixing speed can be tuned by simply changing the switching frequency of pumping.

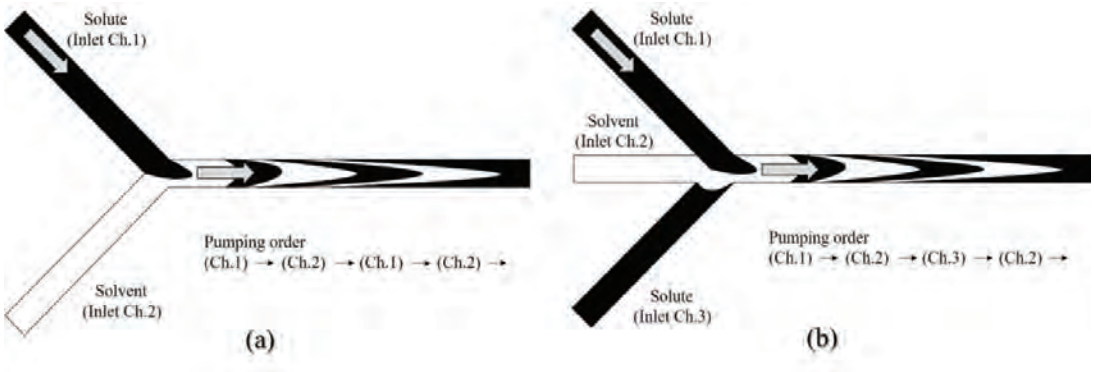

Figure 26 Schematics of the pulsing technique. (a) Y-shaped microchannel, (b) three inlets microchannel.

Performance of the sequential segmentation mixer is reported at different operating conditions. Mainly, six different parameters were tested. Firstly the effect of switching frequency at four switching frequencies was tested. The first case has a 50 Hz frequency, the second is with 100 Hz, the third was 150 Hz, and the fourth case had 200 Hz. All the cases had 50% duty cycle (DC) and an inlet average velocity of 10 mm/s. An additional case without segmentation was performed to show the main advantage of going to sequential segmentation method. Secondly after choosing the best performing frequency over time, the effect of three different averaged velocities is performed. The three cases are 5 mm/s, 10 mm/s, and 15 mm/s. Thirdly after choosing the best performing frequency and averaged velocity over time, the effect of three different duty cycles was performed. The three cases are 50% DC, 25% DC, and 75% DC. The fourth test is for different aspect rations (H:W), the three cases are 4:1, 1:1, and 1:4, they were performed with 50% DC, the best performing frequency, and the best performing averaged velocity. The fifth and sixth parameters to test were the effect of different cross-sectional shapes and configuration of inlet branches. The three cases for the cross-sectional shapes are rectangular, circular, and triangular. For the effect of inlet configuration of inlet branches, the four cases are the Y-shape, T-shape, arrow head shape, and hydrodynamic focusing. These cases were also performed with 50% DC and the best performing frequency in a rectangular microchannel with aspect ratio of 1:1.

4.1 Mixing Analysis

Various indices have been employed to quantify mixing in microfluidic devices to represent the extent of mixing. The mathematical function of the mixing index (MI) involves a measure of standard deviation of the concentration over the cross section of the microchannel [57, 83]. The standard deviation is expressed as follows:

$$\sigma = \sqrt{\frac{1}{N}\sum_{i=1}^{N}(c_i - c_m)^2} \tag{16}$$

where σ is the standard deviation, N is the number of sampling points, c_i is the mixing fraction at point i. and c_m is the optimal mixing fraction at the outlet of the channel.

The use of standard deviation as a measure of mixing, is better than simply using conventional methods like c_{min}/c_{max}, because it explains exacly how all of the points in

the data set are spread, whereas conventional methods that only consider specified points such as maximum and minimum, like the one implied in the validation case do not give the full picture. Therefore, the formula employed in the present study to calculate mixing index (MI), based on the standard deviation of concentration, is expressed as follows [57]:

$$\mathrm{MI} = 1 - \frac{\sigma}{c_m} \tag{17}$$

The value of the mixing index is 0 and 1 for the unmixed and fully mixed states respectively.

4.2 Improvement of mixing using sequential segmentation

The detailed results are presented for two cases, (i) without segmentation (constant flow rates), (ii) with segmentation of the two inlet streams in the Y-shaped rectangular channel with a 150 Hz frequency, 50% DC, and 1:1 aspect ratio. The two cases serve to explain the behavior of mixing inside the microchannel. MI is calculated for all cases at x = 2 mm after 0.6 second from flow initiation. This time was sufficient to flush the liquid initially filling the microchannel and reach a steady state periodic fluctuation of concentration over time inside the microchannel as shown in Figure 27. It will be shown later while discussing the effect of frequency that MI at all frequencies also reached a periodic fluctuating state in similar time.

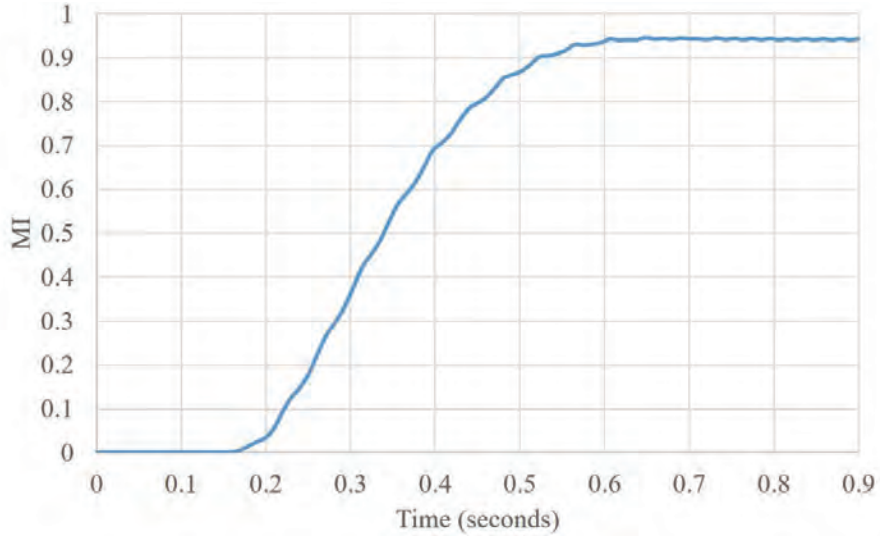

Figure 27 Mixing index for 150 Hz at x= 2 mm with time. The mixing index starts at 0 and then develops until it starts to periodically fluctuate around 0.942 after 0.6s.

The MI was calculated at x = 2 mm for all cases, because this is where all frequencies are fluctuating around a MI of 0.9 and a comparison can be constructed in that shorter region as shown in Figure 28.

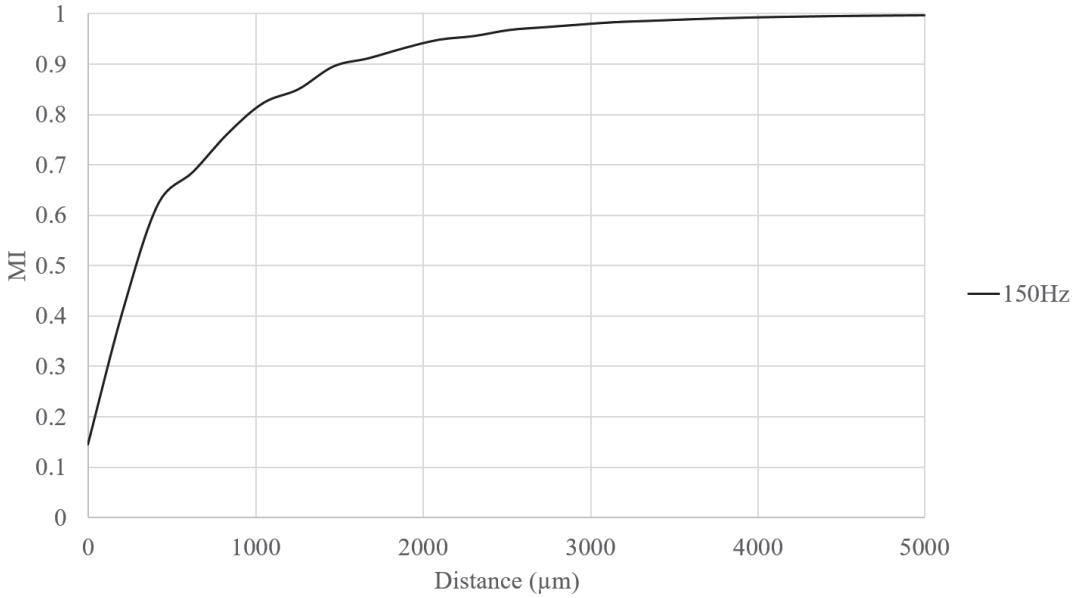

Figure 28 Variation of mixing index with distance for 150 Hz case, following a single injected high concentration pulse from one inlet starting at 0.7s.

The case where there is a constant flow rate of 10 mm/s with no flow segmentation at both inlets is shown in Figure 29. In all color contour levels of the mass fraction, a mass fraction of one is represented by red, thus visualizing solute while a mass fraction of zero is pictured in dark blue, corresponding to the solvent. This figure shows that most of the solute from the upper inlet remains on one side of the channel and most of the solvent remains on the other side, were the mixing zone is confined to a narrow band around the vertical interface, indicating very little mixing of 0.544.

In the second case we seek the improvement of the mixing without altering the geometry of the device, by simply pulsing the flow rate of both inlets, the fully developed average velocity for both inlets is now forced to be as a square wave function (the specific velocity inlet boundaries are indicated in Table 1). Figure 30 includes a time series of images that reveal how the interface between the solvent and solute plugs stretches during a pulse cycle in the YZ-plane and XY-plane.

The interface length increases as the plugs moves downstream the channel leading to enhance mixing due to Taylor-Aris dispersion. This pulsation of the interface increases the extent of mixing, leading to a MI of 0.942 compared to 0.544 for the segmentation-free case.

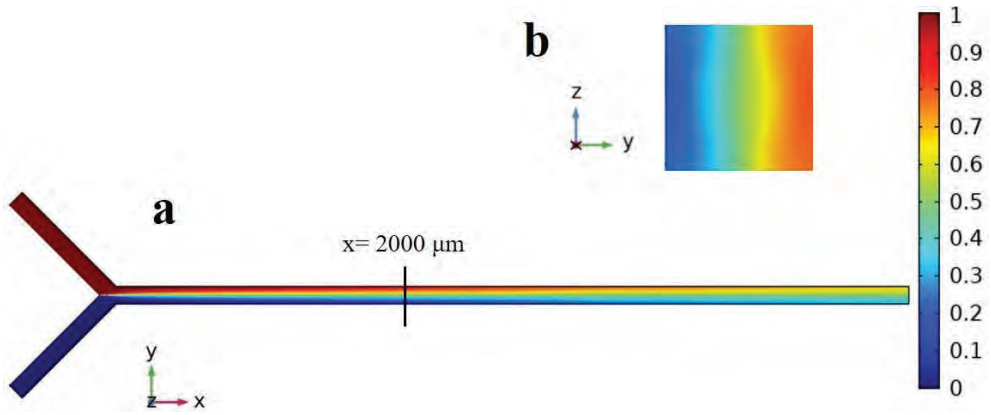

Figure 29 Numerical simulation of constant flow rate in both inlets (no segmentation), (a) in the XY-plane cross-section at half the channel depth and (b) in the YZ-plane cross-section, taken at 2 mm downstream of the confluence.

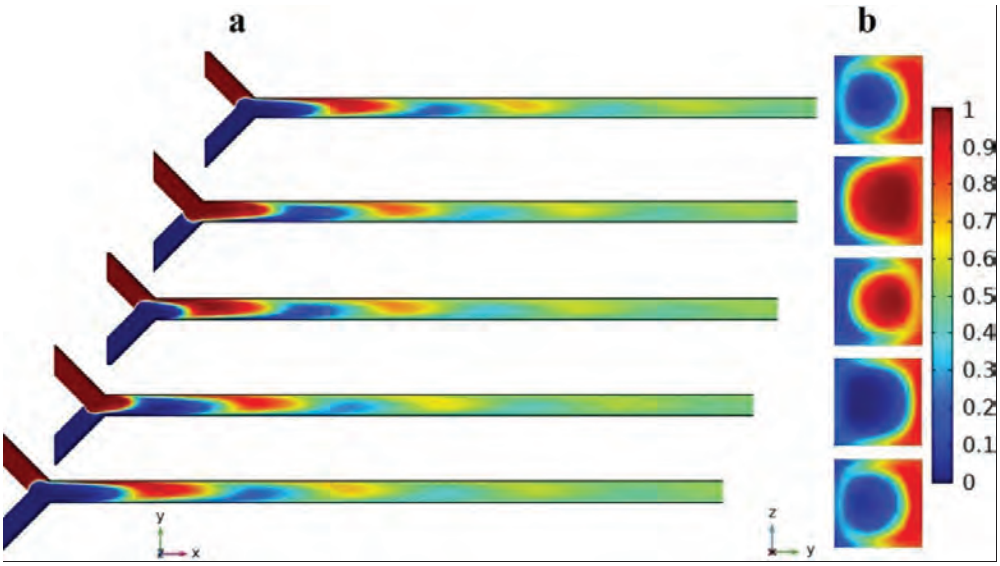

Figure 30 Numerical simulation results obtained with pulsing at the two inlet flows, the time period of the snap shots is 0.042 seconds. (a) XY-plane at half the channel depth, (b) YZ-plane cross-section taken 0.2 mm downstream of the intersection of the two inlets. Notice the formation of a finger-shaped fold in the YZ-plane cross-section and alternative pulses of solute and solvent traveling downstream are clearly visible in the XY-plane.

Although, there is considerable change in the concentration distribution over the channel cross section with time close to the junction between branches, further downstream (2 mm from the junction), there is limited variation in the concentration. The degree of mixing, which is calculated at 2 mm downstream, varies by less than 0.5% through each pulse cycle. Alternative pulses of solute and solvent traveling downstream can be clearly seen in the XY-plane (Figure 30a).

Figure 31 shows the pressure distribution across the microchannel when the same solute pulse is on. It is clearly shown that at the solute inlet channel the pressure is 250 pa above the atmospheric pressure, while at the outlet of the microchannel it is atmospheric pressure. Also Figure 32 shows the Velocity distribution just downstream of the intersection of the two inlets and throughout the channel over the switching period. It is clear that there is a difference in the velocity directly at the junction, while after the Y junction the velocity profile becomes fully developed.

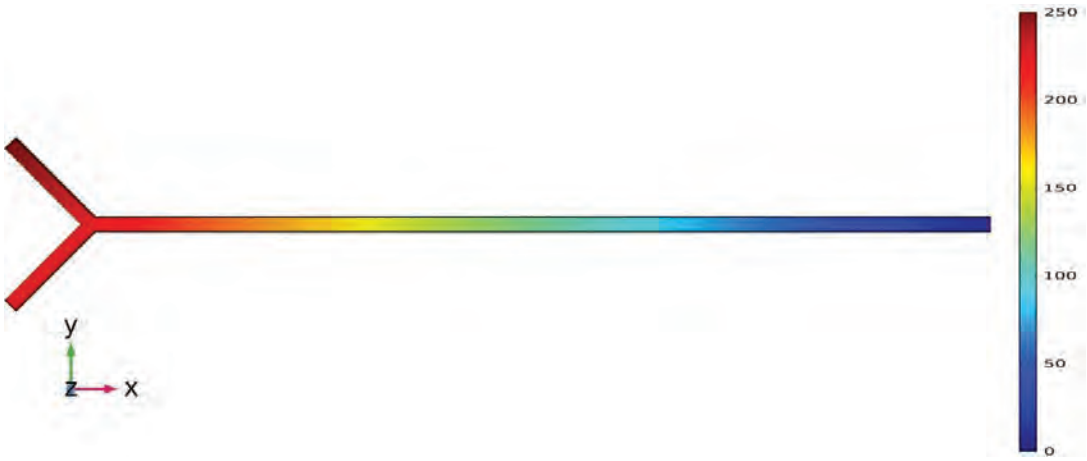

Figure 31 Pressure distribution along the Y-shaped microchannel when the solute is switch on, and the solvent is switched off.

The importance of the velocity and pressure distributions are essential towards understanding why some phenomena's are happening in this study. Where due to pressure difference between the two inlet channels, the segmented pulse from the switch on pulse pushes the switched off pulse as shown by a blue circle in the zoomed segment of Figure 33a. This phenomena is happening in all of the studied cases.

Figure 33b shows the details of the pulsing segments when the solute (red) is switched on at the junction (x = 0 mm directly before the entrance of the main channel). This figure shows how the solute pulse does not cover the full segment of the channel cross-section, which causes a trailing flow between pulses. This is extremely important in the distinction between all of the upcoming cases, where if this trail decreases the MI will increase and vice versa.

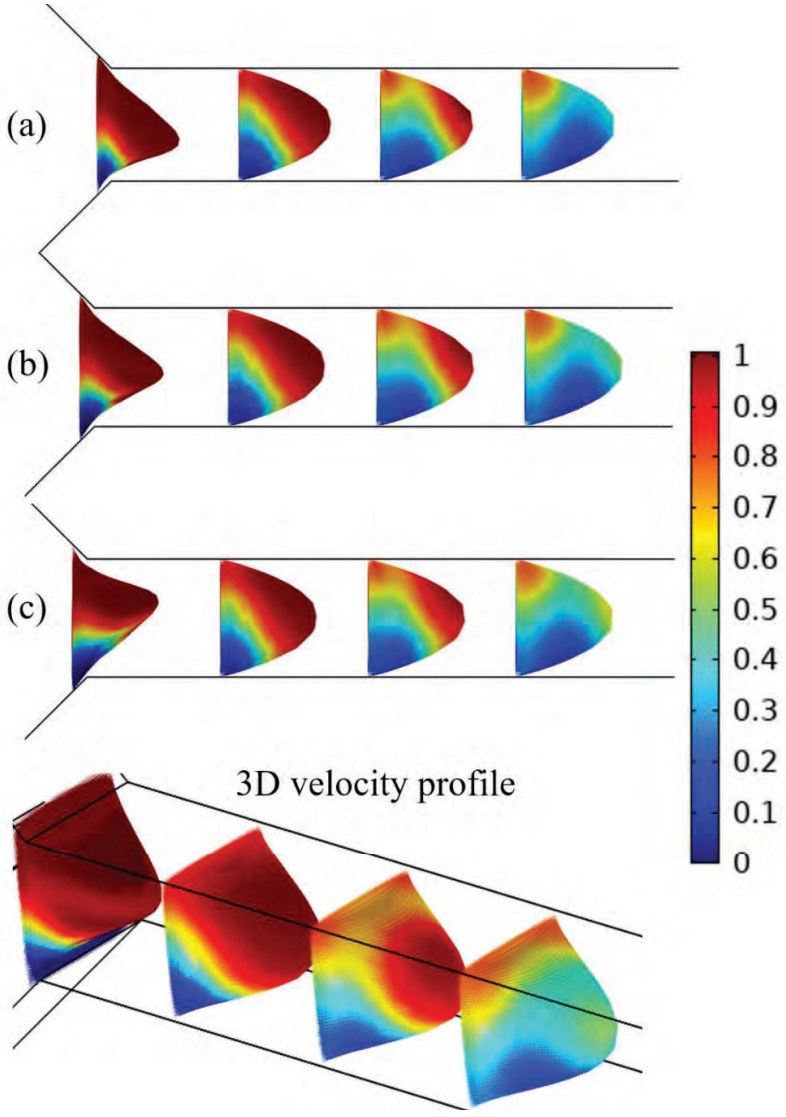

Figure 32 Velocity profile of the sequential segmentation pulse, colors indicate the concentration while vector size indicates velocity magnitude. (a) When the solute is switched on, and the solvent is switched off, (b) during the switching between the pulses, (c) when the solvent is witched on, and the solute is switched off.

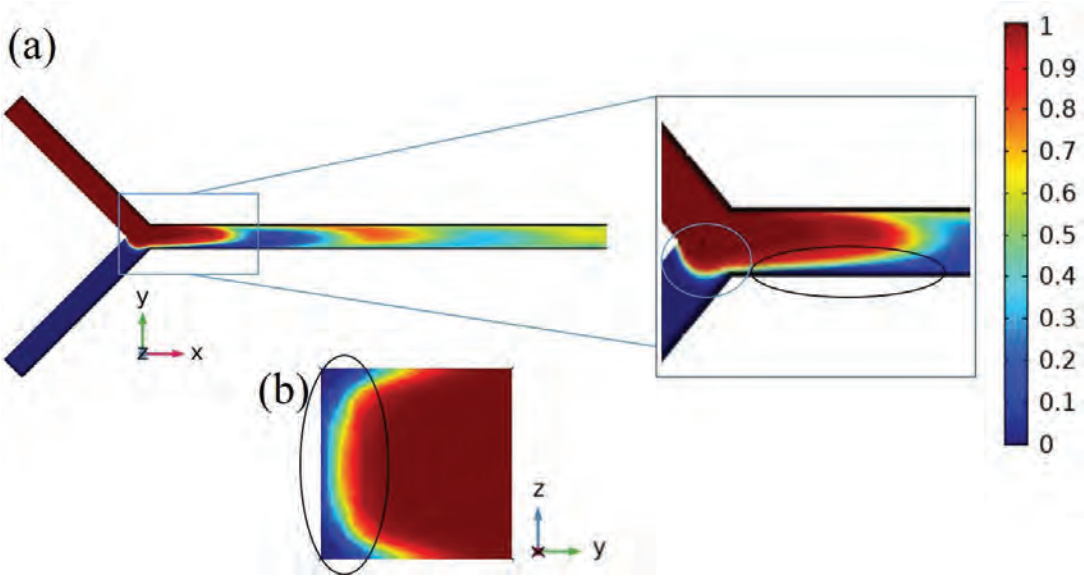

Figure 33 (a) XY-plane of the channel, on the right side a zoomed segment is taken to show the effect of pressure between the two inlet streams in the blue circle and the trailing effect in the black circle.(b) YZ-Plane of the channel at x= 0 mm(directly before the entrance to the main channel), which shows is the black circle how the pulse does not cover the full segment and there is a trailing flow between pulses, Note: The channel is clipped short in X- direction to compact stack the image and this image is taken at the last time step for solutes pulse (Red) to be switched on.

4.3 Effect of Frequency

In this study, the switching frequency for four different cases (50 Hz, 100 Hz, 150 Hz, and 200 Hz) were examined for the 3D Y-shaped microchannel with a 50% duty cycle.

The results are shown in Figures 34 and 35. They correspond to a specified cross section at x = 2 mm after the conversion of the two streams. The results were taken over a time period of 0.12s across the cross-sectional area starting from 0.7s. It can be clearly seen that the highest average MI of 0.942 is achieved when the frequency is set to 150 Hz. The trend shows that by increasing the frequency, MI increases except for the case 200 Hz case. This is happening because at such high frequency, flow is not completely switched off in either inlets when the other inlet is switched on.

The effect of the incomplete switching off appears in the form of a trailing flow of both the solvent and solute along the sidewalls of the mixing channel adjacent to each inlet at higher switching frequencies as shown in Figure 36. The first solution is

not completely switched off when the second solution is switched on, which results in a residual continuous flow of the solution near the sidewall, it is shown with black and blue circles in Figure 36. This significantly decreases the mixing speed, and indicates that increasing the frequency further, results in the reduction of the mixing index.

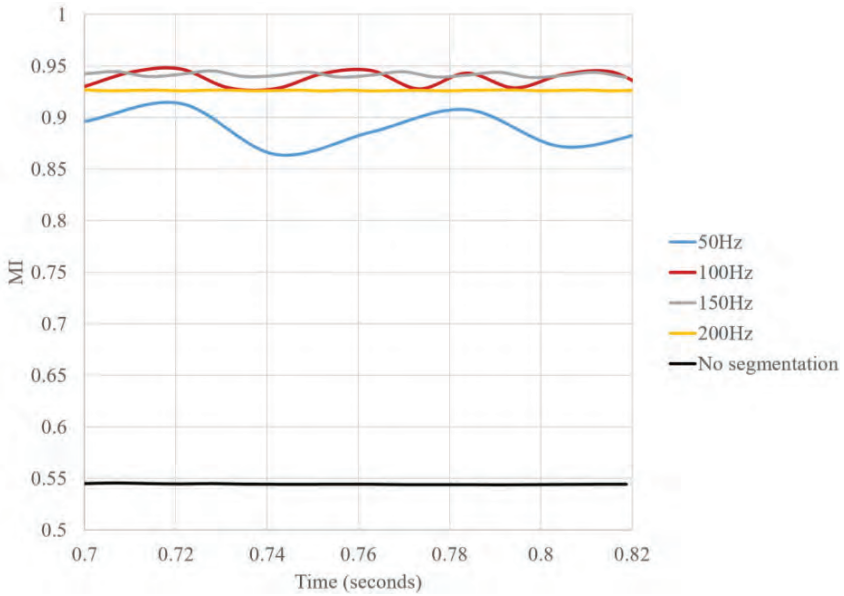

Figure 34 Mixing index for the no segmentation case, and different frequencies over a period of time. These results are examined with 50% DC, 10 mm/s, and (1:1) aspect ratio at x = 2 mm.

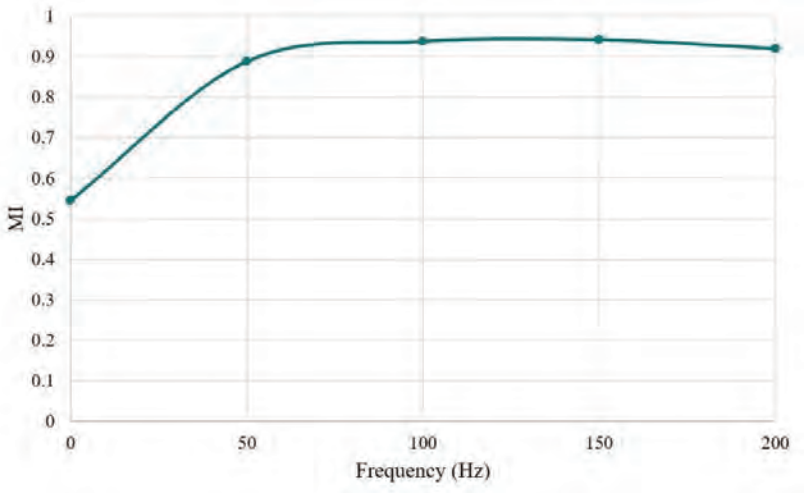

Figure 35 Effect of frequency on the mixing index, with a 50% DC in a cross-section located at x = 2 mm.

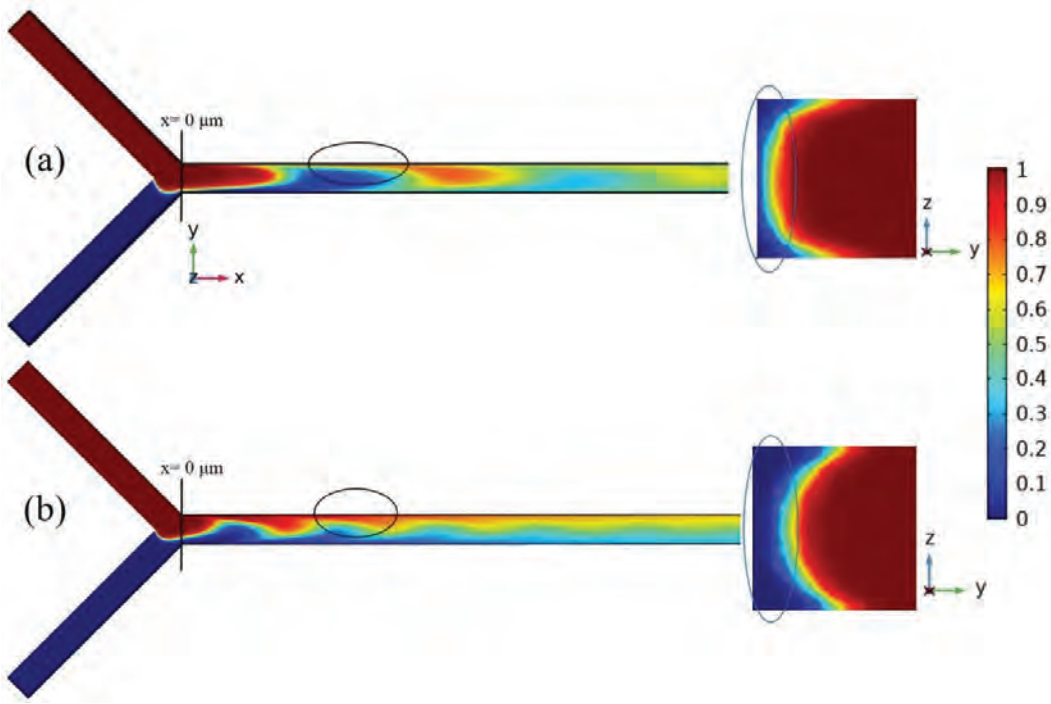

Figure 36 Numerical simulation results obtained with pulsing for two different frequencies at the same time with a cross-sectional view at the junction (x= 0 mm) on the right side. (a) 150 Hz case, (b) 400 Hz case.

4.4 Effect of Flow Velocity

The effect of changing flow velocity is investigated for three different cases, while keeping a fixed frequency of 150 Hz and 50% DC. Changing the averaged velocity from 10mm/s to 15 mm/s and 5 mm/s had a slight decrease of 1.5% and 2.3% respectively in the MI.

In the 15 mm/s case this is happening due to the larger size of each segment (Figure 37a), which indicates the requirement of more time to mix, even when the trailing effect is minimal. By decreasing the velocity to 5 mm/s an incomplete switching similar to the high frequency effect occurs (Figure 37c), which decreases the mixing inside of the microchannel. Figure 38 illustrates all of the MI results for the different cases.

4.5 Effect of Duty Cycle

Duty cycle is the fraction of one period in which the solute is switched on to the duration of the entire period, Figure 39. The duty cycle is expressed as follows:

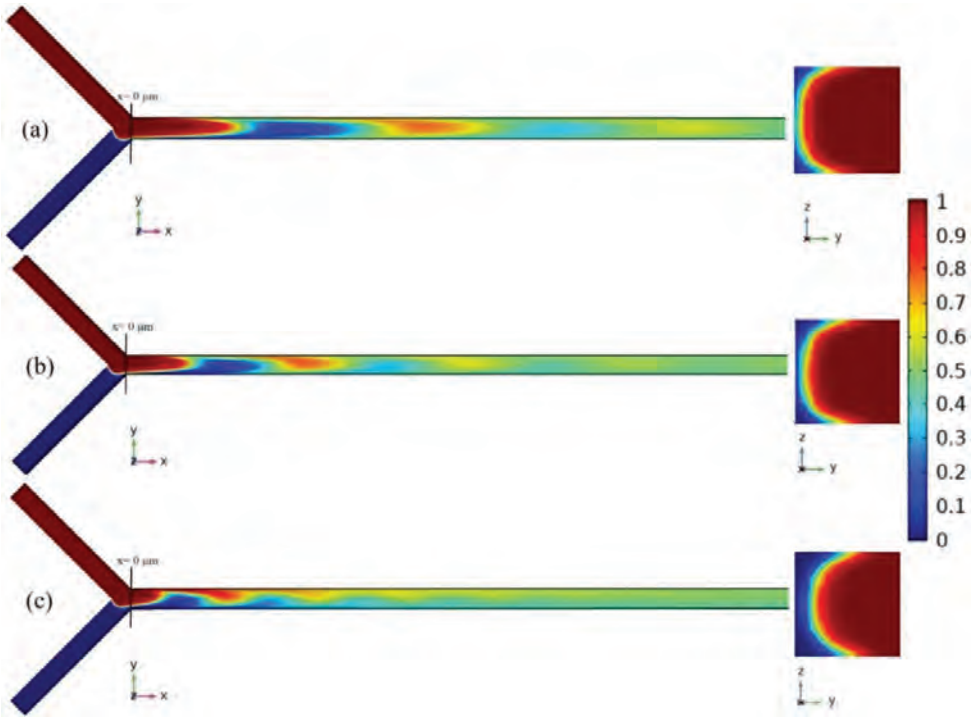

Figure 37 Numerical simulation results obtained with pulsing at 150 Hz,50% DC, and (1:1) aspect ratio for three different averaged velocity in XY-plane and a cross-sectional view at the junction (x= 0 mm) on the right side. (a) 15 mm/s, (b) 10 mm/s, and (c) 5 mm/s.

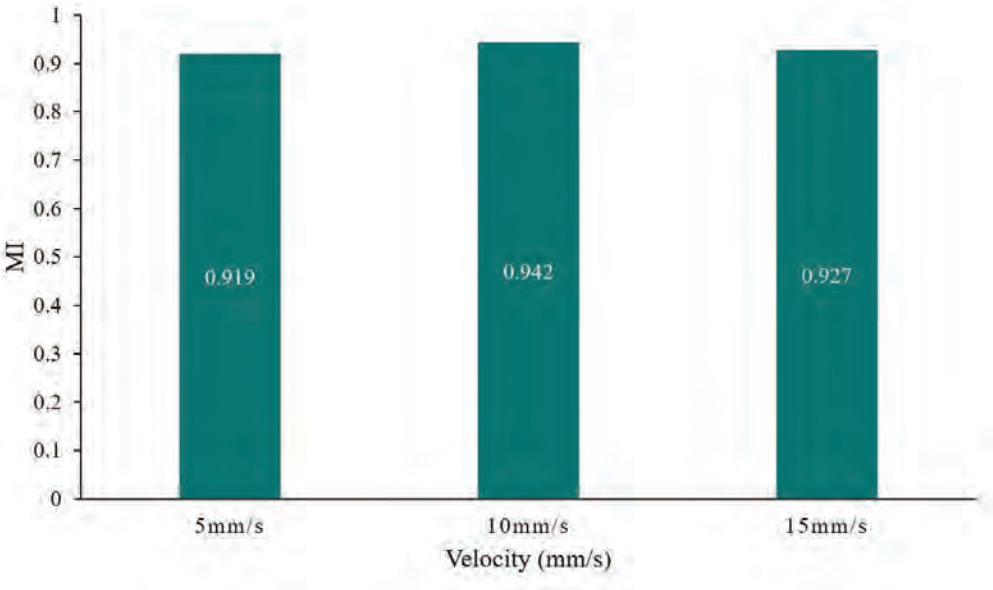

Figure 38 Effect of average velocity on the mixing index, at a constant 150 Hz frequency, 50% DC and (1:1) aspect ratio. The results are obtained at specified cross section located at x = 2 mm.

$$\text{Duty Cycle} = \frac{T_w}{T} \times 100\% \tag{18}$$

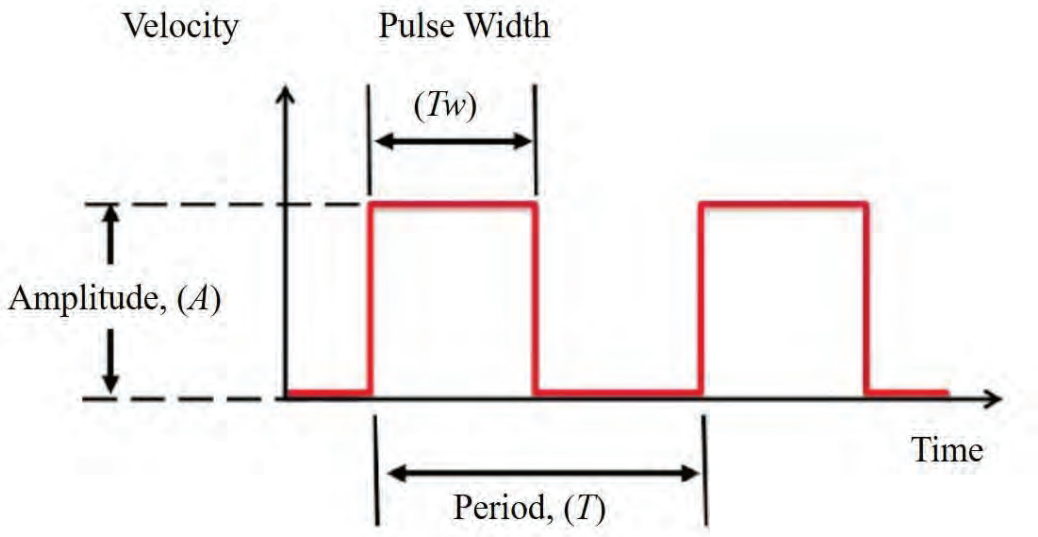

Figure 39 Duty Cycle parameters, T is the period of the pulse, A is the amplitude, Tw is the pulse width.

Different duty cycle ratios are helpful for specific microfluidic applications that require different mixing fractions of the solutions. For example a duty cycle of 50% should be used when the final concentration of the solute in the solvent after complete mixing is desired to be 50%, whereas a duty cycle of 25% should be used when the final concentration desired is 25%.

In this study, three duty cycle ratios were examined for 150 Hz frequency. The results are obtained at the same x location of 2 mm. Variation of the MI over time at different duty cycles is clearly shown in Figure 40, and their averaged MI values are shown in Figure 41. It is clear that by using the 75% duty cycle for the solute the efficiency increased by almost 2%, from the conventional 50% duty cycle. The 25% duty cycle caused a decrease in MI about 6% from the 50% duty cycle. Please note that the optimal concentration c_m used in the formula for calculating MI, equations 16 and 17, was different for each duty cycle. The outlet fully mixed concentration c_m was set as 0.25, 0.5, and 0.75 for duty cycles of 25%, 50%, or 75%, respectively.

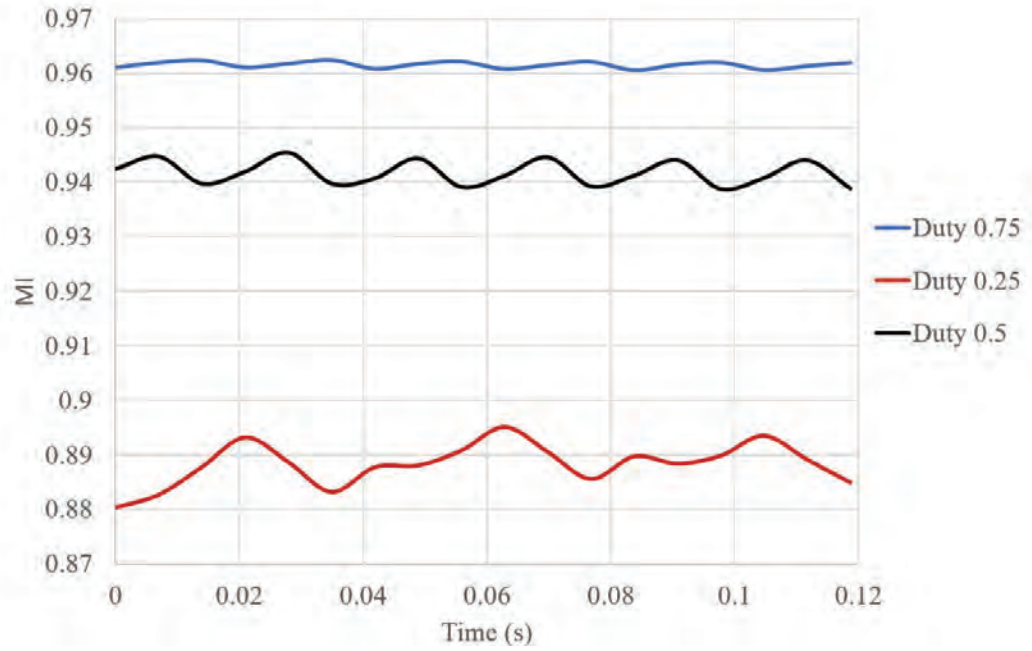

Figure 40 Effect of duty cycle on the mixing index over time, with 150 Hz frequency, and 1:1 aspect ratio. The results are obtained at specified cross section located at x = 2 mm.

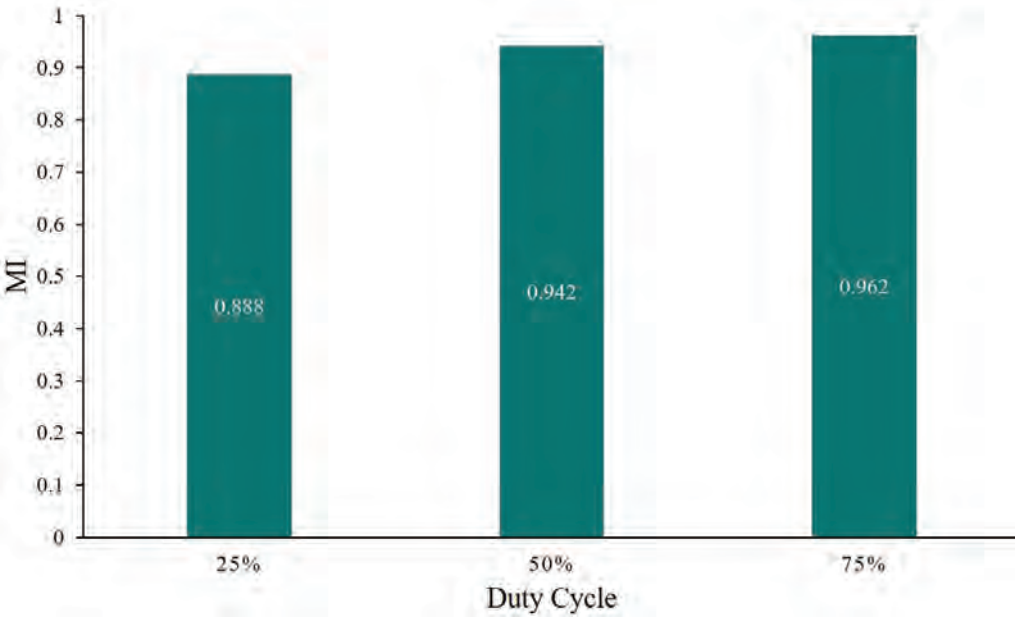

Figure 41 Effect of duty cycle on the mixing index, at a constant 150 Hz frequency. The results are obtained at specified cross section located at x = 2 mm.

4.6 Aspect Ratio

The effect of changing the aspect ratio (H:W) was investigated for three different cases, while keeping a fixed channel cross section area of 6400 μm^2. Changing the aspect ratio from (1:1) to (4:1) had a slight increase of 3% in the MI; this is happening due to the increase of the area of the interface between the two streams, since pulses almost covers the whole cross section of the channel as shown in Figure 42a, whereas by changing the aspect ratio to (1:4), a huge decrease in the MI occurred. This happens due to the decrease in the interfacial surface area between the two solutions, and an incomplete switching of the pulses which results in a residual continuous flow instead of a sequential segmentation as can be seen in Figures 42c.

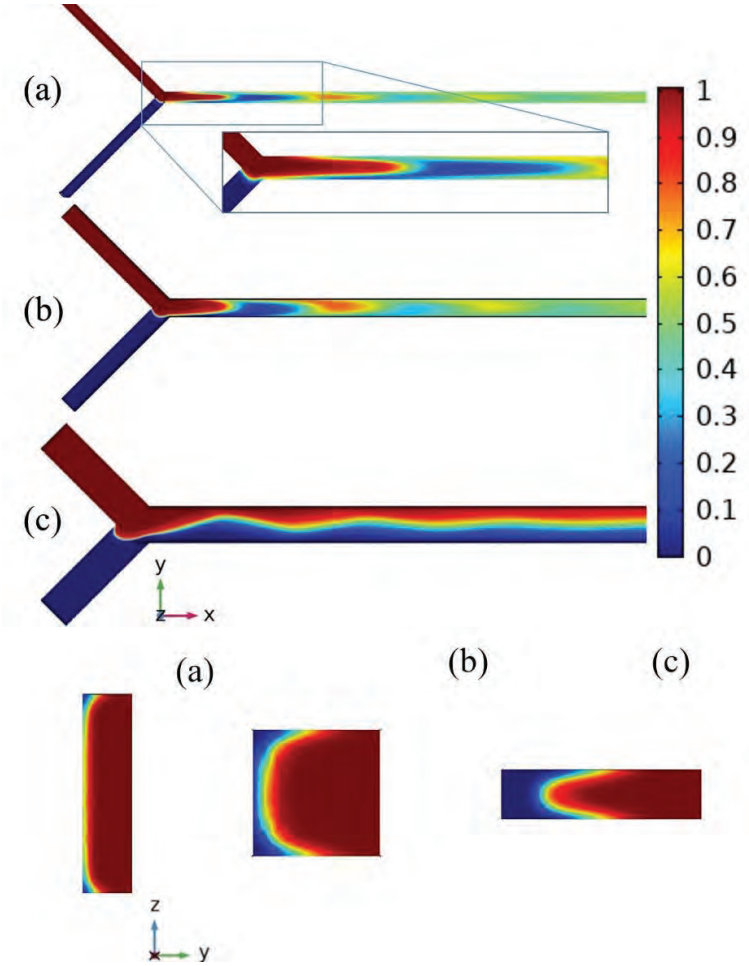

Figure 42 Aspect ratio effect on the concentration with 150 Hz frequency, and 50% DC in XY-plane and across the cross-sectional area YZ-plane, (a) aspect ratio (4:1) with a zoomed part at the junction to show how the pulse almost covers the whole segment, (b) aspect ratio (1:1), and (c) aspect ratio (1:4).

For a wide microchannel, most of the solute from the upper inlet remains on one side of the channel and most of the solvent remains on the other side, with the mixing zone confined to a narrow band around the interface, indicating very little mixing. Figure 43 illustrates all of the MI results for the different cases.

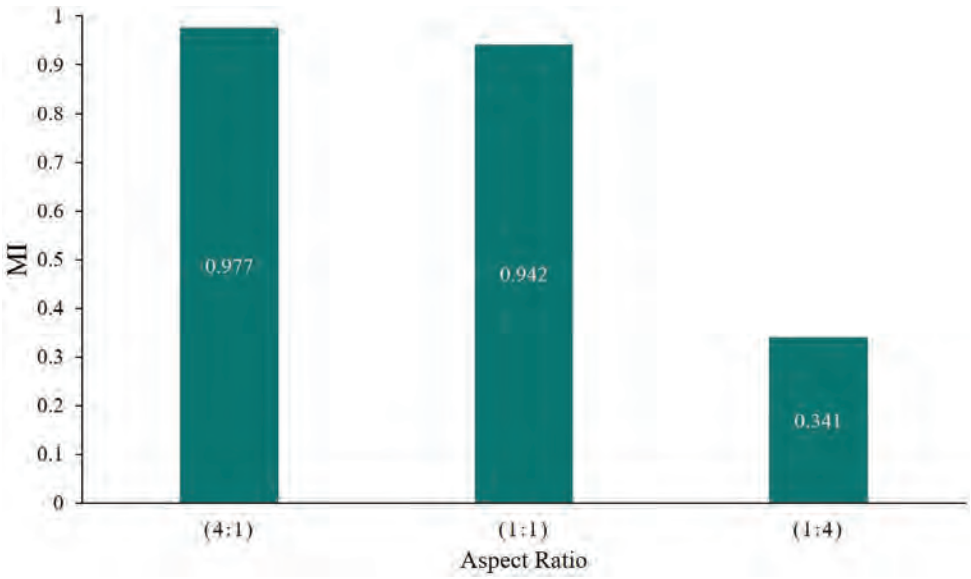

Figure 43 Effect of aspect ratio on the mixing index over a period of time, at a constant 150 Hz frequency and 50% DC. The results are obtained at specified cross section located at x = 2 mm.

4.7 Cross-Sectional Shape

The effect of changing the cross-sectional shape was investigated for three different cases (rectangular, triangular, and circular), while keeping a fixed channel cross-sectional area of 6400 μm^2.

Changing the cross-sectional shape from rectangular to triangular resulted in a slight increase of 2% in the MI; this happens due to the increase of the interfacial surface area and the decrease of the trailing effect as shown in Figure 44, whereas by changing it to circular cross-section, the MI only increase by less than 0.05%. This indicates that there is no need to bear the additional complications for producing circular microchannels, which are difficult to fabricate on the microscale as this does not reflect on mixing improvement.

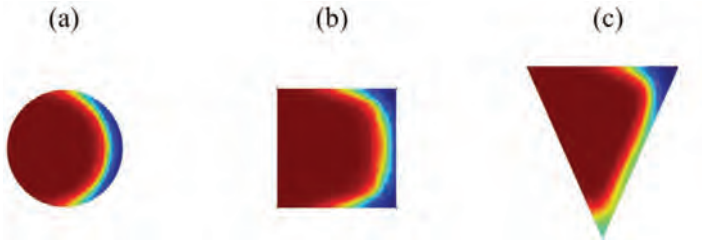

Figure 44 Concentration distribution across the cross-sectional at the junction (x = 0 mm) with 150 Hz and 50% DC at 0.732s. (a) Circular cross-section, (b) rectangular cross-section, and (c) Triangular cross-section.

Figure 45 shows the velocity profile for triangular and circular microchannels, starting from the junction of the channels. It shows the velocity profile variation at the junction during the switching process between solute and solvent pulses, and a 3D view of the velocity profile along the channel. Figure 46 illustrates all of the MI results for the different cases.

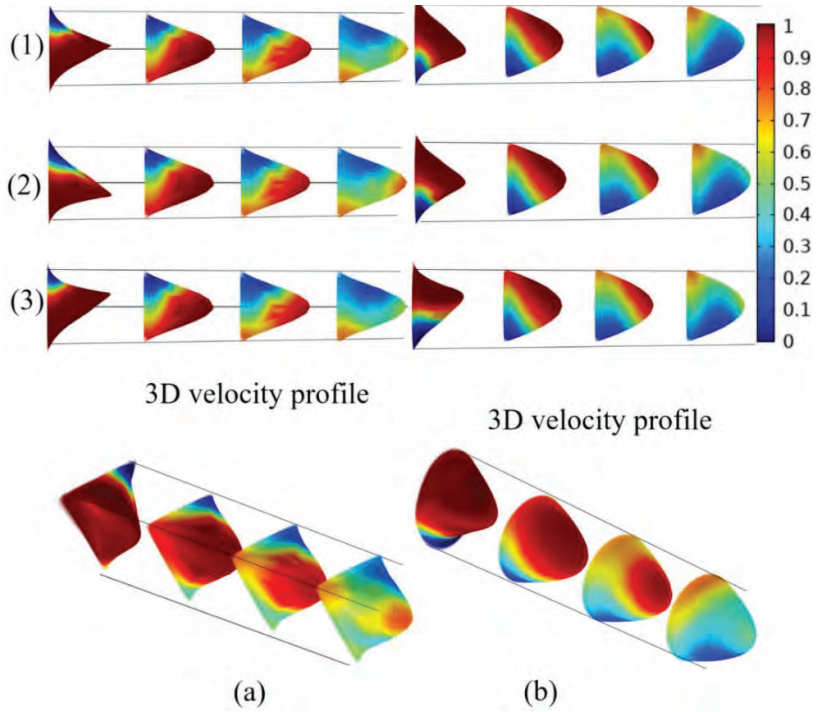

Figure 45 Velocity profile of the sequential segmentation pulse with 150 Hz frequency. (1) Indicates that the solute is switched on, solvent switched off, (2) during the switching between the pulses, (3) when the solvent is switched on, solute is switched off. (a) Triangular microchannel velocity profile, (b) circular microchannel velocity profile.

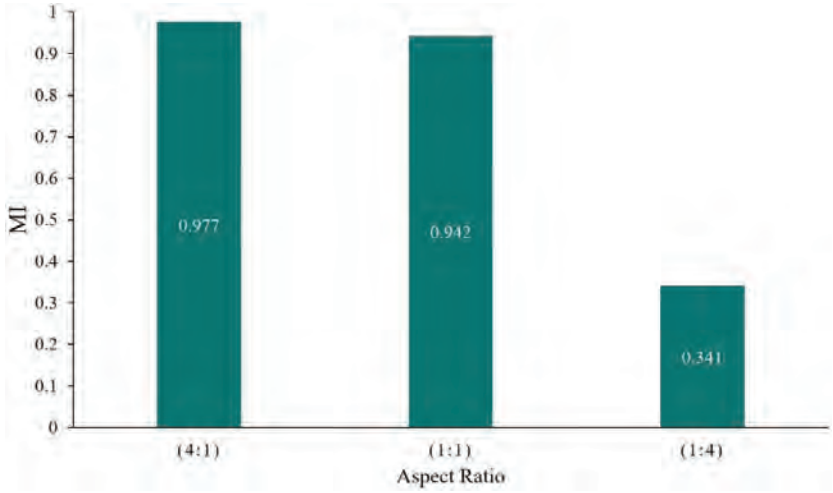

Figure 46 Effect of aspect ratio on the mixing index over a period of time, at a constant 150 Hz frequency and 50% DC. The results are obtained at specified cross section located at x = 2 mm.

4.8 Effect of Inlet Configuration of Inlet Branches

The effect of different inlet configurations of the inlet branches is investigated for four different cases. Figure 47 illustrates all of the MI results for the different cases. It is seen that by changing the Y-shaped inlet branches to T-shape or Arrow head shape leads to a decrease of almost 4% in mixing.

Figures 48 and 49 include a time series of images for T-shape and arrow head shape microchannels. These figures reveal how the interface stretches during a pulse cycle in the YZ-plane and XY-plane, with its curvature being a function of time during the pulse cycle. A finger shape similar to the Y-shaped microchannel is shown, whereas by using the 3 inlets (hydrodynamic focusing) configuration leads to a perfect mixing of 99.7%. This happens due to the combination of the sequential segmentation and hydrodynamic focusing techniques, where by this combination the solute pulse is squeezed between the two solvent pulses, which produces two mixing interfaces as shown in Figure 50. Figure 50a also indicates that the perfect mixing can be further reached downstream of the channel and the extra length of the channel is not required. This configuration also overcomes the undesirable incomplete switching of solutions, which appears along the sidewall of the mixing channel at higher switching frequencies in the two-inlet cases. Since in the hydrodynamic focusing case this effect is desirable,

a further increase in frequency will lead to quicker mixing efficiency and a reduction in the required channel length.

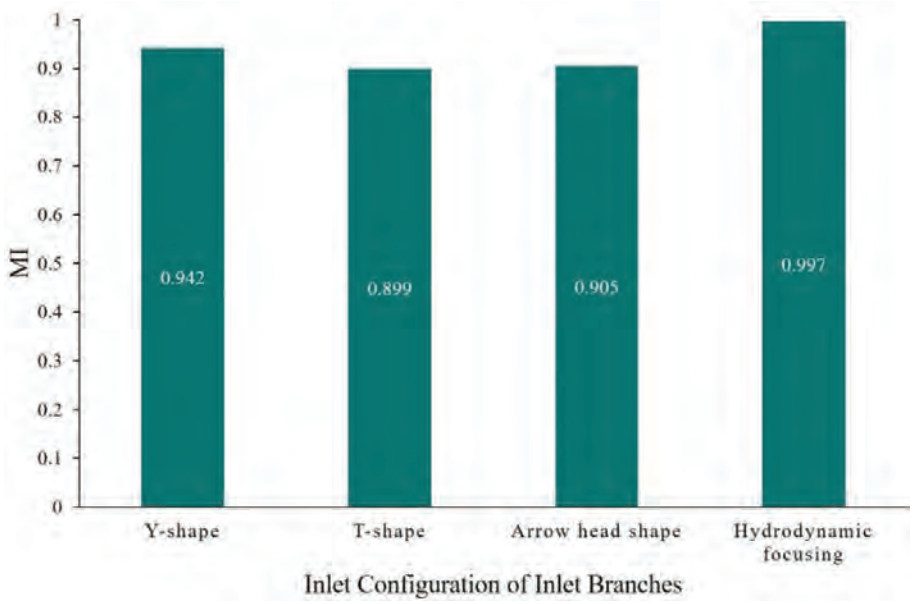

Figure 47 Effect of different inlet configuration of inlet branches on the mixing index over a period of time, at a constant 150 Hz frequency and 50% DC. The results are obtained at specified cross section located at x = 2 mm.

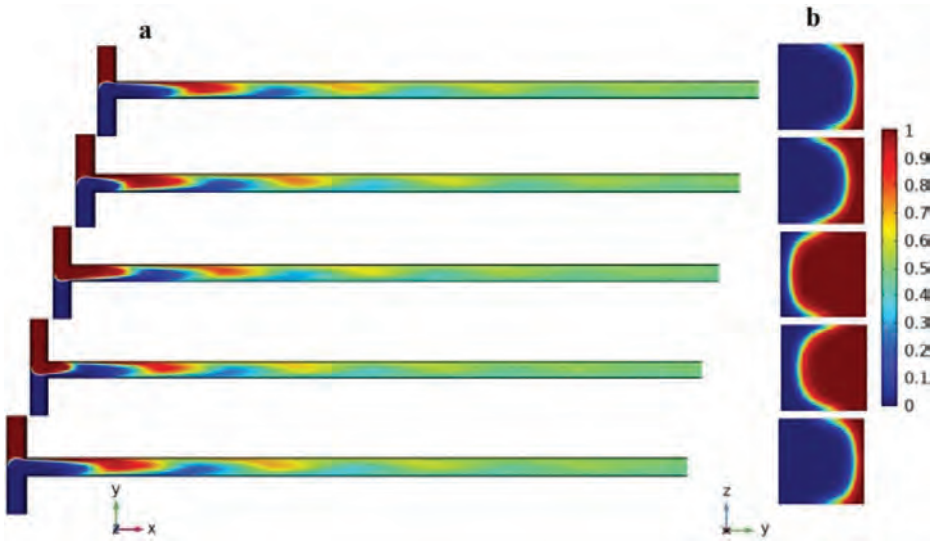

Figure 48 Numerical simulation results obtained with pulsing at the two inlet flows for arrow head shaped microchannel with 150 Hz frequency, 50% DC and 1:1 aspect ratio. The time period of the snap shots is 0.042 seconds. (a) XY-plane cross-section at half the channel depth, (b) YZ-plane cross-section taken at the junction (0 mm).

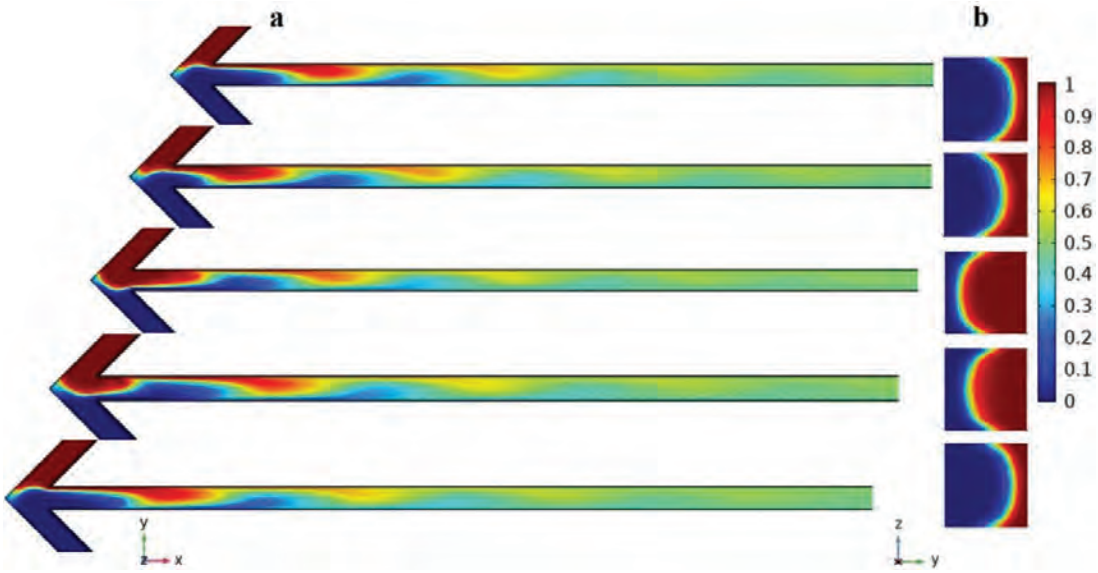

Figure 49 Numerical simulation results obtained with pulsing at the two inlet flows for arrow head shaped microchannel with 150 Hz frequency, 50% DC and 1:1 aspect ratio. The time period of the snap shots is 0.042 seconds. (a) XY-plane cross-section at half the channel depth, (b) YZ-plane cross-section taken at the junction (0 mm).

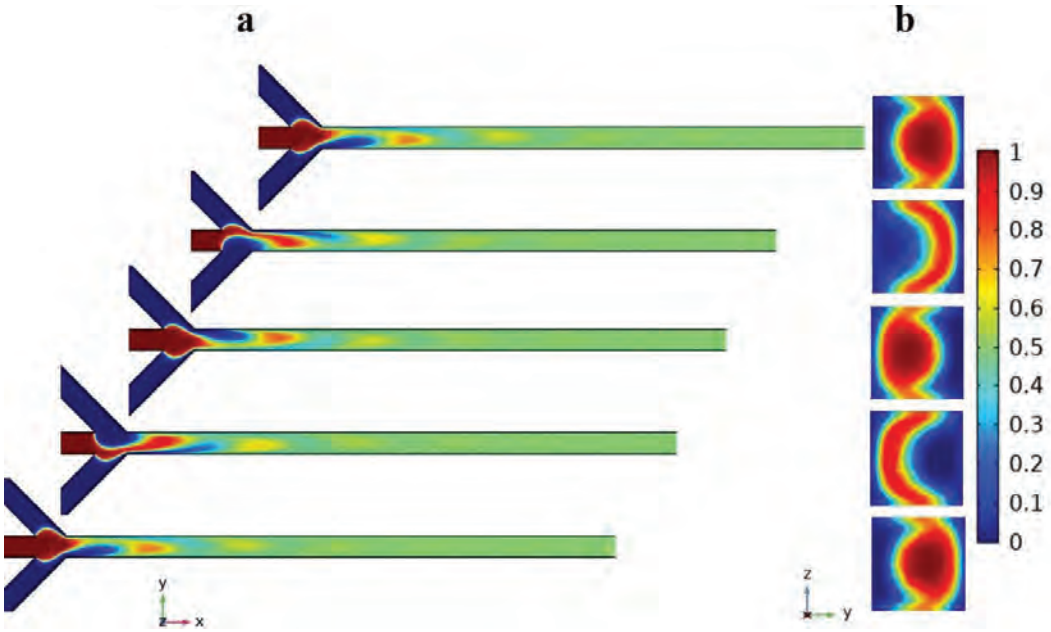

Figure 50 Numerical simulation results obtained with pulsing in the hydrodynamic focusing microchannel with 150 Hz frequency, 50% DC and 1:1 aspect ratio. The time period of the snap shots is 0.042 seconds. (a) XY-plane cross-section at half the channel depth, (b) YZ-plane cross-section taken directly at the entrance of the main channel x= 0 mm. Notice the formation of a squeezed-shaped solute (red) fold in the YZ-plane cross-section between the two solvent pulses. Pulses of solute and solvent traveling downstream are clearly visible in the XY-plane.

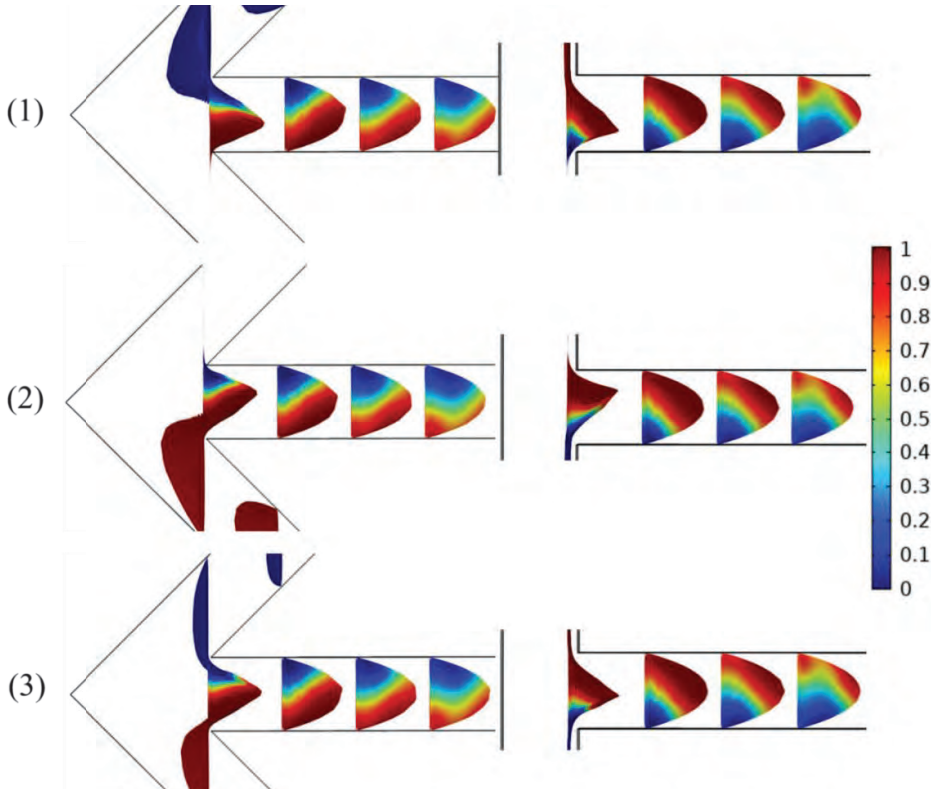

Figure 51 Velocity profiles with 150 Hz frequency. (1) Indicates that the solute is switched on, and the solvent is switched off, (2) during the switching between the pulses, (3) when the solvent is witched on, and the solute is switched off, (a) arrow head shape microchannel, (b) T shape microchannel.

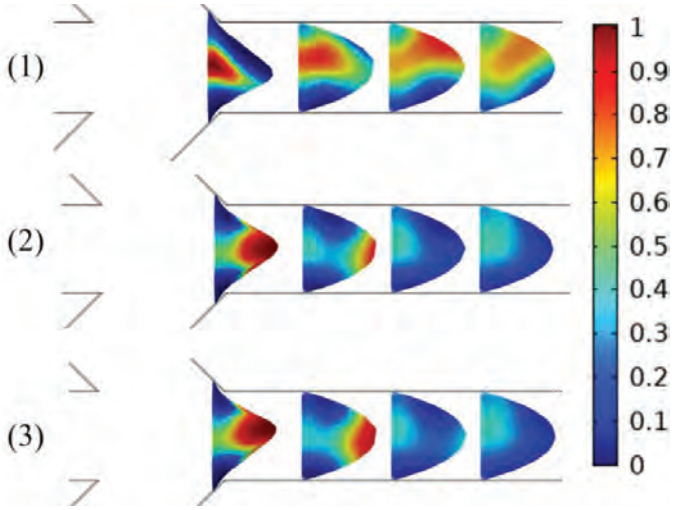

Figure 52 Velocity profile for the hydrodynamic focusing case with 150 Hz frequency. (1) Indicates that the upper solvent is switched on, and the solute is switched off, (2) when the solute is witched on, and the solvent is switched off, (3) indicates that the upper solvent is switched on, and the solute is switched off.

Chapter 5. Conclusion and Future Work

5.1 Conclusion

In this study, a comprehensive model describing the effectiveness of using sequential segmentation as a mixing technique at the microscale level was reported. This model assisted in demonstrating the capability of using a sequential varying flow rates, where it is shown how it provides a significantly better mixing than the conventional constant flow rates at both inlets. The obtained results confirm the capability of sequential segmentation as a good mixing mechanism for various microfluidic applications. The main advantages over other mixing techniques is that it is quicker than passive micromixers and does not require complex structure fabrication. Compared to other active techniques, sequential segmentation can be used in chemical applications such as nanoparticle synthesis. Another advantage of sequential segmentation is that it does not require building any structures to confine the flow inside the microchannel which makes it compatible with biological applications where severe shear stresses on flowing samples (e.g. cells) are to be avoided.

One the other hand, sequential segmentation has its own challenges in terms of applicability. Those challenges mainly appear in the need for high switching frequency micropumps, high response controllers, and creating a perfect switching between segments with different wave functions. The most important thing while using sequential segmentation is to firstly find the optimum calibration and operation conditions for the required geometry and application. An optimization of different microchannel configurations and inlet boundary conditions affecting the mixing is concluded and summarized as follows:

1. Switching frequency has a moderate effect on the mixing index for the two-inlet microchannel. Increasing the frequency from 50 Hz to 150 Hz leads to an increase of 5% in mixing compared to an improvement of 35% when fluctuating flow is compared to constant flow rates at the inlets. It is also shown that by increasing the frequency further the mixing starts to decrease, this happens because of the incomplete switching of solutions which results in a residual continuous flow of the solvent and solutes near the sidewalls.

2. Effect of changing the flow velocity with 150 Hz frequency and 50% DC: by decreasing the averaged velocity from 10 mm/s to 5 mm/s had a decrease of 2.3%. This happens because of the incomplete switching of solutions due to the slow velocity, while increasing the velocity from 10 mm/s to 15 mm/s decreased the mixing index by 1.5%. This happens due to the large size of segments, which requires longer time to mix.
3. Controlling the duty cycle is an efficient method of controlling the final concentration of the solute in the microchannel. However, it has a small effect on the mixing index. Increasing the duty cycle of the solute from 50% to 75% leads to an increase of 2% in mixing. Decreasing it to 25% leads to a decrease of 5.4% in the mixing index.
4. Effect of changing the aspect ratio while keeping the same cross-sectional area: The aspect ratio of 4:1 has a moderate increase of 3%, while the 1:4 decreases the mixing significantly, which is even worse than the constant flow inlets case. This happens due to an incomplete switching of the pulses, which results in a residual continuous flow instead of a sequential segmentation.
5. Changing the cross-sectional shape while keeping the same cross-sectional area, also has a small effect on the mixing index. Changing the cross-sectional shape from rectangular to triangular leads to an increase of 2% in the mixing index, while changing it to circular results in a small increase of only 0.03%.
6. Changing the inlet configuration of the inlet branches has a significant effect on the mixing index. Changing from the Y-shape to three inlets leads to a perfect mixing index of 99.7%, whereas changing the Y-shape to T-shape or arrow head shape leads to a decrease in the mixing index by 4.3% and 3.7% respectively. Mixing improvement in the three-inlet case happens due to the combination of sequential segmentation and hydrodynamic focusing techniques.

5.2 Future Work

The current work presents confirm the potential of sequential segmentation as an efficient microscale mixing technique. However, further studies are needed to make full usage of the technique. Some of the required future studies are suggested below:

1. Study the effect of different velocity profiles such as the case of electroosmotic flow in which the velocity profile is almost uniform.

2. Investigate the effect of different flow viscosities on the mixing index at different frequencies.
3. Soft microchannels at the microscale level may experience different behavior than what is presented here due to the compliance of channel walls and its expansion/contraction when the pressure is increased or decreased. Further numerical simulations are required to study this effect on mixing efficiency.
4. Using sequential segmentation to enhance nanoparticle synthesis inside microfluidics devices. By building a fast-switching pressurized system to induce fast flow segmentation, and use the developed setup to prepare polymeric nanoparticles inside microchannels using sequential segmentation.
5. Investigating the effect of Dean flow in curved microchannels on mixing efficiency of sequential segmentation. Curved microchannels will generate a secondary flow in the plane of the channel cross section due to centrifugal forces, which produces additional vortices in the plane of the microchannel cross section.
6. Investigate the effect of using different wave types such as sinusoidal, sawtooth, triangular, etc. They can be studied with and without reverse flow in the inlet.

References

[1] S. A. Khan, A. Gunther, M. A. Schmidt, and K. F. Jensen, "Microfluidic synthesis of colloidal silica," *Langmuir,* vol. 20, no. 20, pp. 8604-8611, 2004.

[2] R. Karnik *et al.*, "Microfluidic Platform for Controlled Synthesis of Polymeric Nanoparticles," *Nano Letters*, vol. 8, no. 9, pp. 2906-2912, 2008/09/10 2008.

[3] M. Y. He, J. S. Edgar, G. D. M. Jeffries, R. M. Lorenz, J. P. Shelby, and D. T. Chiu, "Selective encapsulation of single cells and subcellular organelles into picoliter- and femtoliter-volume droplets," *Analytical Chemistry,* Article vol. 77, no. 6, pp. 1539-1544, Mar 2005.

[4] D. Di Carlo, L. Y. Wu, and L. P. Lee, "Dynamic single cell culture array," *Lab on a Chip,* vol. 6, no. 11, pp. 1445-1449, 2006.

[5] M. H. Fortier, P. Thibault, E. Bonneil, and P. Goodley, "Integrated microfluidic device for mass spectrometry-based proteomics and its application to biomarker discovery programs," *Analytical Chemistry*, vol. 77, no. 6, pp. 1631-1640, 2005.

[6] N. Honda, U. Lindberg, P. Andersson, S. Hoffmann, and H. Takei, "Simultaneous multiple immunoassays in a compact disc-shaped microfluidic device based on centrifugal force," *Clinical Chemistry,* vol. 51, no. 10, pp. 1955-1961, 2005.

[7] T. Laksanasopin, T. Guo, S. Nayak, A. Sridhara, S. Xie,, "A smartphone dongle for diagnosis of infectious diseases at the point of care," *Science Translational Medicine,* vol. 7, no. 273, pp. 273ref1-1– 273ref1-9, February 4, 2015.

[8] J. Sun, Y. Xianyu, M. Li, W. Liu *et al.*, "A microfluidic origami chip for synthesis of functionalized polymeric nanoparticles," *Nanoscale,* vol. 5, no. 12, pp. 5262-5265, 2013.

[9] D. Liu, S. Cito, Y. Zhang, C.-F. Wang, T. M. Sikanen, and H. A. Santos, "A Versatile and Robust Microfluidic Platform Toward High Throughput Synthesis of Homogeneous Nanoparticles with Tunable Properties," *Advanced Materials,* vol. 27, no. 14, pp. 2298-2304, 2015.

[10] R. Frank, "The SPOT-synthesis technique: Synthetic peptide arrays on membrane supports - Principles and applications," *Journal of Immunological Methods,* vol. 267, no. 1, pp. 13-26, 2002.

[11] A. M. Nightingale and J. C. deMello, "Segmented Flow Reactors for Nanocrystal Synthesis," *Advanced Materials*, vol. 25, no. 13, pp. 1813-1821, 2013.

[12] G. S. Jeong, S. Chung, C. B. Kim, and S. H. Lee, "Applications of micromixing technology," *The Analyst,* vol. 135, no. 3, pp. 460-473, Mar 2010.

[13] R. B Bird, W. E Stewart, and E. Lightfoot, *Transport Phenomena*. 2nd revised ed. Hoboken, NJ: Wiley, 2006.

[14] E. Hovad, "Taylor dispersion in time dependent flow," Master Thesis, Technical University of Denmark, 2011.

[15] R. Aris, "On the Dispersion of a Solute in a Fluid Flowing through a Tube," *Proceedings of The Royal Society A: Mathematical, Physical and Engineering Sciences,* vol. 235, no. 1200, pp. 67-77, 1956.

[16] G. Taylor, "Dispersion of soluble matter in solvent flowing slowly through a tube," *Proceedings of The Royal Society A: Mathematical, Physical and Engineering Sciences,* vol. 219, no. 1137, pp. 186-203, 1953.

[17] D. Dutta and D. T. Leighton, "Dispersion Reduction in Pressure-Driven Flow Through Microetched Channels,", *Analytical Chemistry,* vol. 73, no. 3, pp. 504-513, Feb 1 2001.

[18] N.-T. Nguyen and S. T. Wereley, *Fundamentals and applications of microfluidics.* 2nd revised ed. Boston, MA: Artech House, 2006.

[19] Z. Wu and N.-T. Nguyen, "Convective–diffusive transport in parallel lamination micromixers", *Microfluidics and Nanofluidics,* vol. 1, no. 3, pp. 208-217, Jul 2005.

[20] L. Capretto, W. Cheng, M. Hill, and X. Zhang, "Micromixing Within Microfluidic Devices," *Topics in Current Chemistry,* vol. 304, pp. 27-68, 2011.

[21] A. E. Kamholz, B. H. Weigl, B. A. Finlayson, and P. Yager, "Quantitative Analysis of Molecular Interaction in a Microfluidic Channel: The T-Sensor," *Analytical Chemistry,* vol. 71, no. 23, pp. 5340-5347, 1999.

[22] C. Erbacher, F. Bessoth, M. Busch, E. Verpoorte, and A. Manz, "Towards Integrated Continuous-Flow Chemical Reactors", *Microchimica Acta,* vol. 131, no. 1-2, pp. 19-24, 1999.

[23] C.-H. Lin, C. Tsai, and L.-M. Fu, "A rapid three-dimensional vortex micromixer utilizing self-rotation effects under low Reynolds number conditions", *J Micromech Microeng,* vol. 15, no. 5, pp. 935-943, May 2005.

[24] J. Cha, J. Kim, S. Ryu, J. Park *et al.*, "A highly efficient 3D micromixer using soft PDMS bonding", *J Micromech Microeng,* vol. 16, no. 9, pp. 1778-1782, Sep 2006.

[25] F. Schönfeld, V. Hessel, and C. Hofmann, "An Optimised Split-and-Recombine Micro-Mixer with Uniform “Chaotic” Mixing," *Lab on a Chip,* vol. 4, no. 1, pp. 65-69, Feb 2004.

[26] N.-T. Nguyen, *Mixing in Microscale.* Boston, MA: Springer, 2007.

[27] S. W. Lee, D. Sung Kim, S. S Lee, and T. Hun Kwon, "A split and recombination micromixer fabricated in a PDMS three-dimensional structure", *J Micromech Microeng,* vol. 16, no. 5, pp. 1067-1072, May 2006.

[28] T. Woo Lim, Y. Son, Y. Jeong, D. Yang, H. Kong, K. Lee, and D. Kim, "Three-dimensionally crossing manifold micro-mixer for fast mixing in a short channel length," *Lab on a Chip,* vol. 11, no. 1, pp. 100-103, Jan 7 2010.

[29] D. Di Carlo, "Inertial Microfluidics," *Lab on a Chip,* vol. 9, no. 21, pp. 3038-3046, Nov 7 2009.

[30] A. P Sudarsan and V. Ugaz, "Multivortex micromixing," *Proceedings of the National Academy of Sciences of the United States of America*, vol. 103, no. 19, pp. 7228-7233, May 9 2006.

[31] V. Hessel, S. Hardt, L. Holger, and F. Schönfeld, "Laminar Mixing in Different Interdigital Micromixers: I. Experimental Characterization", *Aiche Journal*, vol. 49, no. 3, pp. 566-577, Mar 2003.

[32] J. M Ottino, *The Kinematics Of Mixing: Stretching, Chaos, And Transport*. Cambridge: Cambridge University Press 1989.

[33] A. Stroock, S. K W Dertinger, A. Ajdari, I. Mezic, H. A Stone, and G. M Whitesides, "Chaotic Mixer for Microchannels," *Science*, vol. 295, no. 5555, pp. 647-651, Jan 25 2002.

[34] S. Hoe Wong, P. Bryant, M. Ward, and C. Wharton, "Investigation of mixing in a cross-shaped micromixer with static mixing elements for reaction kinetics studies," *Sensors and Actuators B: Chemical*, vol. 95, no. 1-3, pp. 414-424, 2003.

[35] H. Wang, P. Iovenitti, E. Harvey, and S. Masood, "Optimizing layout of obstacles for enhanced mixing m microchannels", *Smart Materials and Structures*, vol. 11, no. 5, pp. 662-667, Oct 2002.

[36] A. A. Bhagat, S. Bhagat, and I. Papautsky, "Enhancing particle dispersion in a passive planar micromixer using rectangular obstacles", *J Micromech Microeng*, vol. 18, no. 8, pp. 85005-85009, Aug 2008.

[37] A. A. Bhagat, S. Bhagat, E. T. K. Peterson, and I. Papautsky, "A passive planar micromixer with obstructions for mixing at low Reynolds number", *J Micromech Microeng*, vol. 17, no. 5, pp. 1017-1024, May 2007.

[38] W.-F. Fang and J.-T. Yang, "A novel microreactor with 3D rotating flow to boost fluid reaction and mixing of viscous fluids", *Sensors and Actuators B: Chemical*, vol. 140, no. 2, pp. 629-642, Jul 16 2009.

[39] J. M. Park, D. Sung Kim, T. G. Kang, and T. Hun Kwon, "Improved serpentine laminating micromixer with enhanced local advection", *Microfluidics and Nanofluidics*, vol. 4, no. 6, pp. 513-523, Jun 2008.

[40] D. Sung Kim, S. H. Lee, T. Hun Kwon, and C. Ahn, "A serpentine laminating micromixer combining splitting/recombination and advection," *Lab on a Chip*, vol. 5, no. 7, pp. 739-747, Jul 2005.

[41] L. Wang and J.-T. Yang, "An overlapping crisscross micromixer using chaotic mixing principles", *J Micromech Microeng*, vol. 16, no. 12, pp. 2684-2691, Dec 2006.

[42] S. Jae Kim, Y.-A. Song, P. L Skipper, and J. Han, "Electrohydrodynamic Generation and Delivery of Monodisperse Pico-Liter Droplets Using PDMS Microchip," *Anal Chem*, vol. 78, no. 23, pp. 8011-8019, 2006.

[43] R. M Lorenz, J. S. Edgar, G. Jeffries, and D. T Chiu, "Microfluidic and Optical Systems for the On-Demand Generation and Manipulation of Single Femtoliter-

Volume Aqueous Droplets," *Anal Chem*, vol. 78, no. 18, pp. 6433-6439, Sep 15 2006.

[44] E. Quevedo, J. Steinbacher, and D. McQuade, "Interfacial Polymerization within a Simplified Microfluidic Device: Capturing Capsules," *Journal of the American Chemical Society*, vol. 127, no. 30, pp. 10498-10499, Aug 3 2005.

[45] T. Thorsen, R. Roberts, F. Arnold, and S. R. Quake, "Dynamic Pattern Formation in Vesicle-Generating Microfluidic Device," *Physical Review Letters*, vol. 86, no. 18, pp. 4163-4166, Apr 30 2001.

[46] P. Garstecki, M. J Fuerstman, H. A Stone, and G. M Whitesides, "Formation of droplets and bubbles in a microfluidic T-junction - Scaling and mechanism of break-up," *Lab on a Chip*, vol. 6, no. 3, pp. 437-446, Mar 2006.

[47] L. Yobas, S. Martens, W.-L. Ong, and N. Ranganathan, "High-performance flow-focusing geometry for spontaneous generation of monodispersed droplets," *Lab on a Chip*, vol. 6, no. 8, pp. 1073-1079, Aug 2006.

[48] K. Handique and M. A. Burns, "Mathematical modeling of drop mixing in a slit-type microchannel", *J Micromech Microeng*, vol. 11, no. 5, pp. 548-554, Sep 2001.

[49] H. Song, J. Tice, and R. F Ismagilov, "A Microfluidic System for Controlling Reaction Networks in Time," *Angewandte Chemie (International ed.)*, vol. 42, no. 7, pp. 768-772, Feb 17 2003.

[50] H. Song, M. R Bringer, J. Tice, C. Gerdts, and R. F Ismagilov, "Experimental test of scaling of mixing by chaotic advection in droplets moving through microfluidic channels," *Appl Phys Lett*, vol. 83, no. 12, pp. 4664-4666, Dec 1 2003.

[51] M. R Bringer, C. Gerdts, H. Song, J. Tice, and R. F Ismagilov, "Microfluidic Systems for Chemical Kinetics that Rely on Chaotic Mixing in Droplets," *Philosophical transactions. Series A, Mathematical, physical, and Engineering Sciences*, vol. 362, no. 1818, pp. 1087-1104, May 15 2004.

[52] S. A. Khan, A. Günther, M. A. Schmidt, and K. F. Jensen, "Microfluidic synthesis of colloidal silica," *Langmuir*, vol. 20, no. 20, pp. 8604-8611, 2004.

[53] N.-T. Nguyen and X. Huang, "Modelling, fabrication and characterization of a polymeric micromixer based on sequential segmentation," *Biomedical Microdevices*, vol. 8, no. 2, pp. 133-139, Jun 2006.

[54] A. A. Deshmukh, D. Liepmann, and A. P. Pisano, "Continuous Micromixer with Pulsatile Micropumps," *IEEE Workshop on Solid-State Sensor and Actuator*, Hilton Head, SC, 2000, pp. 73-76.

[55] A. A. Deshmukh, D. Liepmann, A. P. Pisano, and B. Sensor, "Characterization of a MicroMixing, Pumping, and Valving System," Obermeier E. T*ransducers '01 Eurosensors XV*. Springer, Berlin, Heidelberg, 2001.

[56] H. Wang, P. Iovenitti, E. Harvey, and S. Masood, "Mixing of two fluid streams in a microchannel using the Taylor-Aris dispersion effect," D. V. Nicolau and A. P. Lee, Eds., vol. 4937, pp. 158-163, 2002.

[57] I. Glasgow and N. Aubry, "Enhancement of microfluidic mixing using time pulsing", *Lab on a Chip,* vol. 3, no. 2, pp. 114-120, 2003.

[58] K. Sugano, Y. Uchida, O. Ichihashi, H. Yamada, T. Tsuchiya, and O. Tabata, "Mixing speed-controlled gold nanoparticle synthesis with pulsed mixing microfluidic system", *Microfluidics and Nanofluidics,* vol. 9, no. 6, pp. 1165-1174, Dec 2010.

[59] K. Sugano, A. Nakata, T. Tsuchiya, and O. Tabata, "High-speed pulsed mixing in a short distance with high-frequency switching of pumping from three inlets", *J Micromech Microeng,* vol. 25, no. 8, pp. 084033-1– 084033-9, Aug 2015.

[60] C. Tan, M. Tracey, J. B Davis, and I. Johnston, "Continuously variable mixing-ratio micromixer with elastomer valves", *J Micromech Microeng,* vol. 15, no. 10, pp. 1885-1893, Oct 2005.

[61] N.-T. Nguyen and X. Huang, "Mixing in microchannels based on hydrodynamic focusing and time-interleaved segmentation: Modelling and experiment," *Lab on a Chip,* vol. 5, no. 11, pp. 1320-1326, Nov 2005.

[62] A. Dodge, A. Hountondji, M.-C. Jullien, and P. Tabeling, "Spatiotemporal resonances in a microfluidic system," *Physical review. E, Statistical, Nonlinear, and Soft Matter Physics,* vol. 72, no. 5 Pt 2, pp. 056312-1– 056312-5, Nov 2005.

[63] K. F. Lei and W. Li, "A Novel In-Plane Microfluidic Mixer Using Vortex Pumps for Fluidic Discretization," *Journal of The Association for Laboratory Automation,* vol. 13, no. 4, pp. 227-236, 2008.

[64] S. Kim, F. Wang, M. A Burns, and K. Kurabayashi, "Temperature-Programmed Natural Convection for Micromixing and Biochemical Reaction in a Single Microfluidic Chamber," *Anal Chem,* vol. 81, no. 11, pp. 4510-4516, Jun 1 2009.

[65] J.-H. Tsai and L. Lin, "Active microfluidic mixer and gas bubble filter driven by thermal bubble micropump", *Sensors and Actuators A: Physical,* vol. 97-98, pp. 665-671, Apr 1 2002.

[66] A. Darhuber, J. P. Valentino, J. M. Davis, S. M. Troian, and S. Wagner, "Microfluidic actuation by modulation of surface stresses", *Applied Physics Letters,* vol. 82, no. 4, pp. 657-659, Jan 27 2003.

[67] M. Oddy, J. Santiago, and J. C Mikkelsen, "Electrokinetic Instability Micromixing," *Analytical Chemistry,* vol. 73, no. 24, pp. 5822-5832, 2002.

[68] J. Posner and J. Santiago, "Convective instability of electrokinetic flows in a cross-shaped microchannel", *Journal of Fluid Mechanics,* vol. 555, pp. 1-42, May 25 2006.

[69] E. Biddiss, D. Erickson, and D.-D. Li, "Heterogeneous Surface Charge Enhanced Micromixing for Electrokinetic Flows," *Anal Chem,* vol. 76, no. 11, pp. 3208-3213, Jun 1 2004.

[70] J. Deval, P. Tabeling, and H. Chih-Ming, "A dielectrophoretic chaotic mixer," *Proceedings of the IEEE Micro Electro Mechanical Systems (MEMS),* pp. 36-39, 2002.

[71] H.-Y. Lee and J. Voldman, "Optimizing Micromixer Design for Enhancing Dielectrophoretic Microconcentrator Performance," *Anal Chem,* vol. 79, no. 5, pp. 1833-1839, Mar 1 2007.

[72] G. Goet, T. Baier, and S. Hardt, "Micro contactor based on isotachophoretic sample transport," *Lab on a Chip,* vol. 9, no. 24, pp. 3586-3593, Dec 21 2009.

[73] H. Bau, J. Zhong, and M. Yi, "A minute magneto hydro dynamic (MHD) mixer", *Sensors and Actuators B: Chemical,* vol. 79, no. 2-3, pp. 207-215, Oct 15 2001.

[74] J. West, B. Karamata, B. Lillis, J. Gleeson *et al.*, "Application of magnetohydrodynamic actuation to continuous flow chemistry," *Lab on a Chip,* vol. 2, pp. 224-230, 2002.

[75] D. W. Oh, J. S. Jin, J. H. Choi, H. Y. Kim, and J. S. Lee, "A microfluidic chaotic mixer using ferrofluid", *J Micromech Microeng,* vol. 17, no. 10, pp. 2077-2083, Oct 2007.

[76] G. G. Yaralioglu, I. O Wygant, T. C Marentis, and P. Khuri-Yakub, "Ultrasonic Mixing in Microfluidic Channels Using Integrated Transducers," *Anal Chem,* vol. 76, no. 13, pp. 3694-3698, Jul 1 2004.

[77] Z. Yang, S. Matsumoto, H. Goto, M. Matsumoto, and R. Maeda, "Ultrasonic Micromixer for Microfluidic Systems", *Sensors and Actuators A: Physical,* vol. 93, no. 3, pp. 266-272, Oct 15 2001.

[78] L.-S. Jang, S.-H. Chao, M. Holl, and D. Meldrum, "Resonant Mode-hopping Micromixing," *Sensors and actuators. A, Physical,* vol. 138, no. 1, pp. 179-186, Jul 20 2007.

[79] D. Ahmed, X. Mao, J. Shi, B. K. Juluri, and T. J. Huang, "A millisecond micromixer via single-bubble-based acoustic streaming," *Lab on a Chip,* vol. 9, no. 18, pp. 2738-2741, Sep 21 2009.

[80] R. H Liu, J. Yang, M. Pindera, M. Athavale, and P. Grodzinski, "Bubble-induced acoustic micromixing," *Lab on a Chip,* vol. 2, no. 3, pp. 151-157, Aug 2002.

[81] Y. Liu and R. E Ecke, "Hybridization enhancement using cavitation microstreaming", *Analytical Chemistry,* vol. 75, no. 8, pp. 1911-1917, Apr 15 2003.

[82] V. Mengeaud, J. Josserand, and H. Girault, "Mixing Processes in a Zigzag Microchannel: Finite Element Simulations and Optical Study," *Analytical chemistry,* vol. 74, pp. 4279-4286, 2002.

[83] A. Hashmi and J. Xu, "On the Quantification of Mixing in Microfluidics," *Journal of Laboratory Automation,* vol. 19, pp. 488-491, 2014.

[84] E. L. Cussler, *Diffusion: Mass Transfer in Fluid Systems*, 3rd edidtion. (Cambridge Series in Chemical Engineering). Cambridge: Cambridge University Press, 2009.

Appendix of Dimensionless Numbers

The mass diffusivity D, the thermal diffusivity $\alpha = k/\rho C_p$ and the momentum diffusivity (kinematic viscosity) $\nu = \mu/\rho$ all have the same unit of m^2/s. The rations of these three competing transport processes represent a group of dimensionless numbers which are helpful to compare between the molecular diffusion and the other transport process in micromixers.

Fluid flow can be categorized mainly into two flows, laminar and turbulent. Laminar flow can be characterized as a smooth and constant fluid motion, whereas turbulent flow is characterized by its fluctuations and vortices. The ratio between advection transport and momentum transport is called Reynolds number:

$$Re = \frac{\rho U D_h}{\mu} = \frac{U D_h}{\nu}$$

where U is the mean velocity in the flow direction and "D_h is the hydraulic diameter of the channel. The hydraulic diameter of the channel is a characteristic number that depends on the geometry of the channel, and is given by" [3]:

$$D_h = \frac{4A}{P}$$

where A is the cross sectional area and P is the wetted perimeter of the channel.

At high Re, the advective mass transport dominates the momentum transport effects and a turbulent flow occurs. In the turbulent flow system, fluids motion is described to be random in both space and time, and there are advective mass transport in all directions. By contrast, at low Re the opposite happens. The flow is dominated by the momentum transport and characterized by a laminar flow. In a laminar flow, the fluid streams flow parallel to each other and the velocity at any location within the fluid stream does not change with time when its boundary conditions are constant. This indicates that the advection mass transfer happens only in the direction of the fluid flow and mixing can only be achieved by molecular diffusion. Between the laminar and turbulent regions there is a transitional Re range. "Which is expected to be in the range of Re = 1500 – 2500. For microfluidic systems, Re are typically smaller than 100 and the flow is laminar" [3].

Lewis number is the ratio between heat transport and diffusive mass transport:

$$Le = \frac{k}{\rho c D} = \frac{\alpha}{D}$$

Peclet number is the ration between advective mass transport and diffusive mass transport:

$$Pe = \frac{U L_{ch}}{D}$$

where L_{ch} is the characteristic mixing length. Usually Peclet numbers in almost all microfluidics ranges from $100 < Pe < 10{,}000$ [26]. That means, advective mass transport will always dominate over diffusive transport.

Schmidt number is the ration between momentum transport and diffusive mass transport.

$$Sc = \frac{\mu}{\rho D} = \frac{\nu}{D}$$

Fourier number is the average diffusion time over the characteristic mixing length. It is also called the striation thickness and it is defined by [84].

$$Fo = \frac{D t_{diff}}{L_{mixing}^2}$$

Vita

Ibragim Abu Dagga was born in 1994, in Volgograd, in Russia. He was educated in local public schools in the United Arab Emirates and graduated from Al Mutanabbi School in 2013. He received a Scholarship to the University of Sharjah in Sharjah, United Arab Emirates, from which he graduated, in 2018. His degree was a Bachelor of Science in Mechanical Engineering.

Directly after graduating in 2018, Ibragim began a Master's program in Mechanical Engineering at the American University of Sharjah.